Chin. Ann. Math.
30B(5), 2009, 539–568
DOI: 10.1007/s11401-009-0102-9

Chinese Annals of Mathematics, Series B

Two-Way Interactions Between Equatorially-Trapped Waves and the Barotropic Flow***

James FERGUSON* Boualem KHOUIDER** Maryam NAMAZI*

(*Dedicated to Professor Andrew Majda on the Occasion of his* 60*th Birthday*)

Abstract Lateral energy exchange between the tropics and the midlatitudes is a topic of great importance for understanding Earth's climate system. In this paper, the authors address this issue in an idealized set up through simple shallow water models for the interactions between equatorially trapped waves and the barotropic mode, which supports Rossby waves that propagate poleward and can excite midlatitude teleconnection patterns. It is found here that the interactions between a Kelvin wave and a fixed meridional shear (mimicking the jet stream) generates a non-trivial meridional velocity and meridional convergence in phase with the upward motion that can attain a maximum of about 50%, which oscillates on frequencies ranging from one day to 10 days. When, on the other hand, the barotropic flow is forced by slowly propagating Kelvin waves a complex flow pattern emerges; it consists of a phase-locked barotropic response that is equatorially trapped and that propagates eastward with the forcing Kelvin wave and a certain number of planetary Rossby waves that propagate westward and toward the poles as seen in nature. It is suggested here that the poleward propagating waves are to some sort of multi-way resonant interaction with the phase locked response. Moreover, it is shown here that a numerical scheme with dispersion properties that depend on the direction perpendicular to the direction of propagation, namely the 2D central scheme of Nessyahu and Tadmor, can artificially alter significantly the topology of the wave fields and thus should be avoided in climate models.

Keywords Equatorially trapped waves, Wave interactions, Jet stream, Rossby waves, Phase locked, Dispersion relation, Central scheme, Climate modeling
2000 MR Subject Classification 65M06, 65M12, 76B15, 76B55, 76B60, 86A10

1 Introduction

Most of the Earth's energy intake from the sun is absorbed within the tropical belt and then redistributed to midlatitudes and polar regions through various atmospheric flow patterns and ocean currents. The energy is transferred from the heated sea-surface to the tropical atmosphere by means of latent heat associated with phase changes of water due to convection. Tropical convection is organized onto a hierarchy of scales ranging from the individual clouds of a few kilometers and one to two hours, to clusters of clouds of a few hundreds of kilometers

Manuscript received March 31, 2009. Published online August 25, 2009.
*Department of Mathematics and Statistics, University of Victoria, Victoria, British Columbia, Canada.
**Corresponding author. Department of Mathematics and Statistics, University of Victoria, PO BOX 3045 STN CSC Victoria, British Columbia, Canada. E-mail: khouider@uvic.ca
***Project supported in part by the Natural Sciences and Engineering Research Council of Canada (No. 288339-2004) and the Canadian Foundation for Climate and Atmospheric Sciences (No. GR-7021).

and one to two days, to superclusters of a few thousands of kilometers and five to 10 days, to their intra-seasonal/planetary scale envelopes of a few tens of thousands kilometers and 40 to 60 days, known as the Madden-Julian oscillation (see [8, 15–17, 28, 36, 37, 45, 57, 58, 65]). Detailed analysis of out-going longwave radiation (OLR), viewed from satellite, combined with shipborne radar data, in the Indian Ocean/Western Pacific warm pool, reveal that the superclusters are the moist-equivalent of the equatorially trapped waves-solutions to the linear rotating shallow water equations on the equatorial beta-plane (see [14, 38, 43, 50]), though with a significantly reduced phase speed and significant discrepancies in the vertical structure (see [40, 55, 57, 65]). Such moisture loaded waves are commonly known as convectively coupled waves. Cumulus parametrizations that are used to capture the non-trivial two-way interactions between the resolved-large scale wave dynamics and the unresolved-small scale convective processes, in climate and weather prediction models, represent poorly the MJO and convectively coupled waves in general (see [11, 30, 32, 33, 44, 46, 49, 52–54, 68]). Idealized models of intermediate complexity, with a simplified dynamical core, that take into account some of the key features of organized convection such as the cloud morphology and moisture variations, on the other hand, do capture qualitatively some important physical and dynamical structure of convectively coupled waves (see [21–25, 29, 40–42]).

Many observational studies demonstrated that the MJO has a profound impact on tropical and extra-tropical weather and climate systems. It can affect the strength and initiation of El-Nino, monsoons, and tropical cyclones as well as several midlatitude weather patterns and storm activity (see [6, 18, 68] and the references therein). Several floods and droughts in the North-Western United states and British Columbia were associated with MJO activity in the tropics (see [6]). The analysis of Roundy [51] suggested non-trivial interactions between the MJO envelopes and convectively coupled Kelvin waves as well as the triggering of poleward propagating Rossby waves during the passage of a Kelvin wave. Both of these phenomena can be attributed to non-linear advective non-linearities as it is observed in the former case that Kelvin waves behave differently during different phases of the MJO (see [51]).

Simple models reduced to one or two shallow water-like systems are commonly used to study nonlinear wave interactions and interactions between tropical waves and extra-tropical teleconnection patterns (see [4, 5, 13, 19, 20, 26, 27, 39, 56, 60–63, 67]). Particularly, the model proposed by Biello and Majda [4, 5, 39] and utilized in [26, 27] is derived from the hydrostatic-Boussinesq primitive equations through a systematic Galerkin projection onto the two first modes of vertical structure: a vertically uniform mode, known as the barotropic mode, and a first baroclinic mode with a half sine/cosine vertical profile. This, in fact, constitutes a minimal model to study nonlinear interactions between equatorially trapped waves that are directed coupled to organized convection and planetary Rossby waves that can propagate poleward and excite teleconnection and midlatitude weather patterns. Early intermediate model convective parametrizations are based on the first baroclinic mode as the main direct heating mode and the barotropic mode mostly as a secondary-advective mode (see [41, 47, 59]).

Biello and Majda [39] used asymptotic expansion to build a solitary-like planetary-scale wave-solution for the coupled barotropic-baroclinic model by exploiting some near-resonant interactions between equatorially trapped waves and barotropic/planetary Rossby waves. Khouider and Majda [27] then conducted a numerical experiment to test the validity of this solution

by integrating the full non-linearly interacting barotropic-baroclinic model forward in time. Interestingly, it is found in [27] that the numerical solution remained both qualitatively and quantitatively similar to the asymptotic solution for a short period of about 2 days, after which energy started to cascade to small scales and a strong energy exchange between the barotropic and baroclinic components of the flow takes place; under the constraint of conservation of total energy, energy is pumped back and forth between the barotropic and the baroclinic modes. The shear complexity of the solution made it impossible to tell which wave or mode is excited by which, although the solitary-wave initial condition consisted of purely baroclinic and barotropic Rossby waves in near-resonant interactions on a significantly large scale, compared to the grid size. Therefore, it is meaningful to break the problem down to two pieces in order to isolate and treat the two-way interactions separately. In other words, it is interesting to know how a prescribed barotropic flow can affect equatorially trapped waves in general and how equatorially trapped waves can in return feedback onto the barotropic flow. This is the purpose of this paper.

Although previous studies suggested that a prescribed background shear (both vertical and meridional) has very little effect on Kelvin waves but very much so on other equatorially trapped waves such as Rossby and mixed-Rossby gravity waves (see [60–63, 67]), here we are primarily interested in the effect of a barotropic shear on Kelvin waves. We do this both for simplicity — because the Kelvin wave is by far the simplest prototype equatorially trapped wave — therefore constitute an easy test bed for our numerical code, and for the fact that Kelvin waves form the bulk part of the observed spectrum of organized tropical convection at synoptic scales. In fact, the zonal structure of observed Kelvin waves display significant deviations from their theoretical-free analogues. For instance, free Kelvin waves in theory have no meridional flow and the y-component of the Coriolis force is exactly balanced by the North-South pressure gradient while the observed Kelvin waves seem to have a weak but non-trivial meridional flow providing extra-North-South convergence of mass and moisture within the region of heating (see [51, 65]). Below we demonstrate that such a meridional flow for the "Kelvin wave" can be generated by the interaction with a barotropic-meridional shear.

Furthermore, previous studies of tropical and extra-tropical teleconnection patterns concentrated mainly on resonant interaction between westward propagating equatorial and barotropic Rossby waves (see [4, 5, 39]) or to the indirect response of the barotropic flow to a prescribed steady heat source in sheared background flow (see [20]). However, the observational analysis of Roundy [51] suggested that an eastward propagating convectively coupled wave in the Indian Ocean initiates Rossby waves that propagate poleward. Therefore the second question addressed here is whether an eastward propagating Kelvin wave can excite such barotropic Rossby solely through advection nonlinearities.

On a more technical side, in our quest for numerical schemes with good balanced features to preserve exactly the geostrophic balance in the meridional direction thus the zero-meridional velocity for the free Kelvin wave, we demonstrate here that an inadequate numerical scheme, with bad dispersive properties, such as the central scheme of Nessyahu and Tadmor [48] can alter significantly the structure of the Kelvin wave in the long run.

The rest of the paper is organized as follows. In Section 2, we present the derivation of the fully coupled barotropic-baroclinic model equations, following [4, 5, 39]. In Section 3, we freeze

the barotropic mode and concentrate on the effect of a barotropic shear on Kelvin waves. We introduce two new variables representing the geostrophic imbalance and rewrite the advected equatorial shallow water equations in terms of these variables for both to highlight the effect of a barotropic shear on a Kelvin wave and for the design of a numerical scheme that in principle preserves exactly the meridional geostrophic balance for the free Kelvin waves, provided that a mass conserving numerical scheme is used. It turns out that this constraint of preserving exactly the meridional geostrophic balance for the Kelvin wave, the simplest conservative scheme (the central scheme of Nessyahu and Tadmor [48]), distorts greatly the structure of the wave in order to balance a serious defect in the central scheme due to the dependence of the numerical phase speed in the zonal direction on latitude. The response of the barotropic equations to an eastward-zonally propagating Kelvin wave is addressed in Section 4. For a more accurate representation of the phase speed of the resulting Rossby waves, the barotropic equations are solved by the celebrated numerical scheme of Arakawa [1], known in the atmosphere/ocean community as the Arakawa Jacobian, which preserves exactly energy and enstrophy. Finally, a concluding summary is given in Section 5.

2 The Barotropic-Baroclinic Model Equations

We consider the primitive equations on the equatorial beta-plane with rigid lid boundary conditions (see [4, 5, 26, 27, 38, 39, 56])

$$\begin{aligned}
&\frac{\mathrm{D}\mathbf{V}_H}{\mathrm{D}t} + \beta y \mathbf{V}_H^{\perp} = -\nabla_H P + \mathcal{S}_{\mathbf{v}},\\
&\mathrm{div}_H \mathbf{V}_H + u_z = 0,\\
&\frac{\mathrm{D}\Theta}{\mathrm{D}t} + \frac{N^2\theta_0}{g} W = \mathcal{S}_{\Theta},\\
&\frac{\partial P}{\partial z} = g\frac{\Theta}{\theta_0},\\
&W|_{z=0,H_T} = 0,
\end{aligned} \tag{2.1}$$

where $\mathbf{V}_H = (U, V)$ is the horizontal velocity, W is the vertical velocity, P is the pressure, and Θ is the potential temperature. Capital letters are used in order to distinguish quantities represented by the primitive equations from their Galerkin projection components which are introduced below. Notice that in (2.1), according to the Boussinesq approximation, the density is assumed to be constant, and the equations are normalized accordingly, except for the buoyancy acceleration in $(2.1)_4$, where, in addition, the hydrostatic balance and the ideal gas law are used. Here $N = 0.01\ \mathrm{s}^{-1}$ is the Brunt-Vaisala buoyancy frequency, $g = 9.8\ \mathrm{m}\cdot\mathrm{s}^{-2}$ is the gravitational acceleration, and $\theta_0 = 300$ K is a reference (constant background) potential temperature while $\beta = 2.2804 \times 10^{-11}\ \mathrm{s}^{-1}\cdot\mathrm{m}^{-1}$ is the gradient of the Coriolis force at the equator. Also

$$\frac{\mathrm{D}}{\mathrm{D}t} \equiv \frac{\partial}{\partial t} + U\frac{\partial}{\partial x} + V\frac{\partial}{\partial y} + W\frac{\partial}{\partial z}$$

is the material derivative, while div_H and ∇_H are the horizontal divergence and horizontal gradient, respectively, while $\mathbf{V}_H^{\perp} = (-V, U)$ and $\mathcal{S}_{\mathbf{v}}$, $\mathcal{S}_{\theta}$ represent sources and sinks of momentum and heat respectively, e.g., Rayleigh friction and convective heating and/or radiative cooling. These forcing terms are set to be zero in the reminder of this paper.

When the primitive equations are Galerkin projected onto the barotropic (i.e., vertically uniform) and a first baroclinic mode, by assuming the crude approximations (see [4, 5, 26, 39, 41])

$$\begin{aligned}\begin{pmatrix}\mathbf{V}_H\\ P\end{pmatrix}(x,y,z,t) &\approx \begin{pmatrix}\overline{\mathbf{v}}\\ \overline{p}\end{pmatrix}(x,y,t)+\begin{pmatrix}\mathbf{v}\\ p\end{pmatrix}(x,y,t)\cos\Big(\frac{\pi z}{H_T}\Big),\\ \begin{pmatrix}W\\ \Theta\end{pmatrix}(x,y,z,t) &\approx \begin{pmatrix}w\\ \theta\end{pmatrix}(x,y,t)\sin\Big(\frac{\pi z}{H_T}\Big),\end{aligned} \tag{2.2}$$

the following coupled barotropic and baroclinic systems of equations are obtained (see [4, 5, 26, 39]):

$$\begin{aligned}&\frac{\partial\overline{\mathbf{v}}}{\partial t}+\overline{\mathbf{v}}\cdot\nabla\overline{\mathbf{v}}+y\overline{\mathbf{v}}^{\perp}+\nabla\overline{p}=-\frac{1}{2}(\mathbf{v}\cdot\nabla\mathbf{v}+\mathbf{v}\operatorname{div}\mathbf{v})=-\frac{1}{2}\operatorname{div}(\mathbf{v}\otimes\mathbf{v}),\\ &\operatorname{div}\overline{\mathbf{v}}=0\end{aligned} \tag{2.3}$$

and

$$\begin{aligned}&\frac{\partial\mathbf{v}}{\partial t}+\overline{\mathbf{v}}\cdot\nabla\mathbf{v}-\nabla\theta+y\mathbf{v}^{\perp}=-\mathbf{v}\cdot\nabla\overline{\mathbf{v}},\\ &\frac{\partial\theta}{\partial t}+\overline{\mathbf{v}}\cdot\nabla\theta-\operatorname{div}\mathbf{v}=0.\end{aligned} \tag{2.4}$$

The equations in (2.3) and (2.4) are non-dimensionalized according to the following reference scales [26, 38, 41]. The gravity wave speed $c=\frac{NH_T}{\pi}\approx 50\ \mathrm{m}\cdot\mathrm{s}^{-1}$ is the velocity scale, the equatorial Rossby deformation radius $L_R=(c\beta^{-1})^{\frac{1}{2}}\approx 1500$ km is the length scale, $T=\frac{L}{c}\approx 8$ hours is the time scale, and $\overline{\alpha}=\frac{H_T N^2\theta_0}{\pi g}\approx 15$ K is the temperature scale.

Note that the vertical velocity and the baroclinic component of pressure are easily recovered through the continuity and hydrostatic balance equations, respectively (see [26]): $w=-\frac{H_T}{\pi}\operatorname{div}\mathbf{v}$ and $p=-\frac{gH_T\theta}{\pi\theta_0}$.

Note that, interestingly, if the nonlinear terms on the right-hand side of equations (2.3) and (2.4) were set to zero, we obtain two independent systems of shallow water equations that both support linear wave solutions. A barotropic system with planetary Rossby waves that can propagate poleward and a first baroclinic system that supports a more complex spectrum of waves that are trapped in the vicinity of and propagate along the equator (see [14, 38, 50]). To appreciate these differences we give here two such simple solutions, one for each one of the decoupled systems. Note that because of the divergence constraint the barotropic system can be rewritten in terms of the vorticity and the stream function

$$\frac{\partial\overline{\xi}}{\partial t}+\overline{u}\frac{\partial\overline{\xi}}{\partial x}+\overline{v}\frac{\partial\overline{\xi}}{\partial y}=-\frac{1}{2}\Big(\Big(\frac{\partial^2}{\partial x^2}-\frac{\partial^2}{\partial y^2}\Big)(uv)+\frac{\partial^2}{\partial x\partial y}(v^2-u^2)\Big) \tag{2.5}$$

with

$$\Delta\overline{\psi}=\overline{\xi}-y,\quad \overline{u}=-\overline{\psi}_y,\quad \overline{v}=\overline{\psi}_x.$$

It is easy to see that, when the baroclinic forcing term on the right-hand side of (2.5) is dropped, $\overline{\psi}(x,y,t)=\mathrm{e}^{\mathrm{i}(kx+ly-\overline{\omega}t)}$ with $\overline{\omega}=-\frac{k}{\sqrt{l^2+k^2}}$ form a family of (linear) wave solutions, known as the planetary Rossby waves (see [38]), which can propagate zonally westward and in both northward and southward directions depending on the values of the wavenumbers k and l.

The simplest free wave solution for the baroclinic system (2.4) in the absence of a barotropic wind ($\overline{\mathbf{v}}=0$) is obtained when the meridional velocity v is set to zero and $u=-\theta$. This yields the well-known equatorial Kelvin wave with $u(x,y,t)=f(x-ct)\mathrm{e}^{-\frac{y^2}{2}}$ (and $\theta=-u$, $v=0$),

which moves eastward along the equator at the gravity wave speed c, introduced above as the velocity unit, and its structure is confined in the vicinity of the equator with an e-folding distance that is proportional to the Rossby deformation radius L_R used here as our length scale. Many other such equatorially-trapped waves are supported by the free-baroclinic system. They go by names such as equatorial Rossby, gravity, and mixed Rossby-gravity of Yanai waves (see e.g. [14, 38, 50] for details). These other waves have a much more complicated meridional structure than the Kelvin wave, but they are all modulated by the same Gaussian $\mathrm{e}^{-\frac{y^2}{2}}$ to remain equatorially trapped. But as it is already mentioned in the introduction, the Kelvin wave happens to be responsible for a large portion of precipitation and kinetic energy due organized tropical convection at the synoptic scale (see [51, 65]). The mixed Rossby-gravity and the Rossby and gravity waves of low meridional index bear the rest of the spectrum power at this scale (see [65]). Simple parametrization models mimicking the observed structure and cloud morphology of organized tropical convective systems that capture qualitatively these convectively coupled waves can be found in [24, 25] and references therein.

Furthermore, we note that, with the appropriate boundary conditions, the coupled system in (2.3) and (2.4) conserves total energy $E_T(t) = \iint(|\overline{\mathbf{v}}|^2 + |\mathbf{v}|^2 + \theta^2)\mathrm{d}x\mathrm{d}y$, where the integral is taken over the computational domain (e.g., a channel along the equator, see [26, 39]), and that when the interaction terms on the right-hand sides are set to zero, the two decoupled systems conserve their own energies (see [26]). Therefore, those interaction terms constitute the only possible means through which the barotropic and baroclinic systems can exchange energy with each other. This feature has been exploited in [26] to design a numerical method with a minimal ad hoc dissipation of energy. As noted in the introduction, it is demonstrated in [27] that when the asymptotic solitary wave-like solution of Biello and Majda [39] was fed into this numerical scheme, vigorous manifestation of energy exchange between the baroclinic and barotropic modes takes place with energy being pumped back and forth between the two modes at a time scale of three to six days. The mechanisms that set these time scales are unclear and it is the goal of this present work to help elucidate some of these complex two-way interactions. The strategy adopted here is to simply freeze in time one of the modes and to force constantly the other mode in a setup that is much simpler. Precisely, we consider the effect of a perpetual meridional (barotropic) shear on Kelvin waves and the response of the barotropic system to a Kelvin wave forcing. Although simplistic in appearance, these two cases have very important practical implication as noted in the introduction.

3 The Effect of a Barotropic Shear on Kelvin Waves

Here, we consider the evolution of a Kelvin wave in a meridional shear environment. Since Kelvin waves and equatorially trapped waves in general play an important role in organized tropical convective superclusters, the issue of the effect of a background shear on these waves has been the focus of many research papers during the past few decades (see [60–63, 67]). However, it has been argued in most of these works (such as [62, 67]) that the effect of the background shear on Kelvin waves is negligible and past studies have been concentrated mostly on mixed Rossby-gravity, Rossby, and westward gravity waves. Though, observed Kelvin waves display a non-trivial meridional velocity and meridional convergence, unlike its theoretical counterpart

where these quantities are exactly zero. The origin of this meridional wind deviation and its effect on the dynamics of the waves remain unexplored. Here we demonstrate by numerical tests that such a nontrivial meridional wind for the theoretical Kelvin wave can be generated through the interactions of a Kelvin wave with a prescribed meridional shear mimicking the equatorial jet stream, with easterlies at the equator and westerlies in midlatitudes around $\pm 30^\circ$ similar to the background wind used in [62, 67] to mimic the climatology over the Eastern Pacific Ocean. When the barotropic wind is reduced to a pure constant shear flow

$$\overline{\mathbf{v}} = (\overline{u}(y), 0), \tag{3.1}$$

where $\overline{u}$ is the barotropic velocity in the zonal direction and y is the north-south distance from the equator, the baroclinic system takes the form

$$\begin{aligned} &\frac{\partial u}{\partial t} + \overline{u}(y)\frac{\partial u}{\partial x} - \frac{\partial \theta}{\partial x} - yv = -v\frac{\partial \overline{u}(y)}{\partial y}, \\ &\frac{\partial v}{\partial t} + \overline{u}(y)\frac{\partial v}{\partial x} - \frac{\partial \theta}{\partial y} + yu = 0, \\ &\frac{\partial \theta}{\partial t} + \overline{u}(y)\frac{\partial \theta}{\partial x} - \frac{\partial u}{\partial x} - \frac{\partial v}{\partial y} = 0. \end{aligned} \tag{3.2}$$

For all practical purposes, this system can be regarded as a forced system of linear-conservation laws (or advection equations) whose solution can in principle be approximated easily by any good numerical method for balance laws (see [2, 3, 7]).

3.1 Exactly balanced numerical scheme for Kelvin waves

Note that when $\overline{u}(y) = 0$, the Kelvin wave solution introduced above satisfies geostrophic balance in the meridional direction: $-\frac{\partial \theta}{\partial y} + yu = 0$. In [26], the F-wave method for balance laws of Bale et al [3] was adapted for the advected baroclinic system in (2.4) (without the interaction terms on the right hand side) in order to capture and preserve this meridional geostrophic balance for the Kelvin wave for instance with good accuracy. Well balanced schemes for conservation laws with forcing aim to capture with high accuracy any small deviations from steady state. The F-wave method in particular is designed so that numerical steady states are exactly preserved to machine precision and therefore can be used to enforce an additional constraint on the governing equations such as the hydrostatic balance or the meridional geostrophic balance for the case of a Kelvin wave. However, unless some clever discretization for the flux term is utilized a steady state (or any other constraint such as the geostrophic balance in y) for the continuous equations is not necessarily preserved after discretization:

$$-\frac{\partial \theta}{\partial y} + yu = 0 \nRightarrow -\widehat{\partial}_y \theta + yu = 0,$$

where $\widehat{\partial}_y$ stands for the numerical derivative of some sort. Nevertheless, the validation experiments conducted in [26] demonstrated that the induced deviation from meridional geostrophy and the resulting meridional velocity for the discretized Kelvin wave remained reasonably small as the system is integrated over relatively long periods of time, perhaps all because of the good balanced properties of the F-wave scheme. However, since a weak meridional shear is expected to distort weakly the geostrophic balance for the Kelvin wave and therefore induce a weak but

non-zero meridional wind, it is highly desirable to eliminate the deviation from geostrophy at the initial time that are due to discretization errors. To this end we introduce the following auxiliary variables that essentially measure the geostrophic imbalance in the meridional direction and therefore the deviations from the Kelvin wave-background solution. Let

$$q = yu - \frac{\partial \theta}{\partial y} \quad \text{and} \quad r = y\theta - \frac{\partial u}{\partial y}.$$

Notice that both q and r are zero in the case of a Kelvin wave solution. Therefore the baroclinic system in (2.4) can be relaxed in terms of the new variables to the five-equations system

$$\begin{aligned}
&\frac{\partial u}{\partial t} + \overline{\mathbf{v}} \cdot \nabla u - \frac{\partial \theta}{\partial x} - yv = -\mathbf{v} \cdot \nabla \overline{u},\\
&\frac{\partial v}{\partial t} + \overline{\mathbf{v}} \cdot \nabla v + q = -\mathbf{v} \cdot \nabla \overline{v},\\
&\frac{\partial \theta}{\partial t} + \overline{\mathbf{v}} \cdot \nabla \theta - \Big(\frac{\partial u}{\partial x} + \frac{\partial v}{\partial y}\Big) = 0,\\
&\frac{\partial q}{\partial t} + \overline{\mathbf{v}} \cdot \nabla q - \frac{\partial \overline{\mathbf{v}}}{\partial y} \cdot \nabla \theta - \frac{\partial r}{\partial x} = -\frac{\partial^2 v}{\partial y^2} + y^2 v + \overline{v}u + v\overline{u} - \mathbf{v} \cdot \nabla(\overline{u}y),\\
&\frac{\partial r}{\partial t} + \overline{\mathbf{v}} \cdot \nabla r - \frac{\partial \overline{\mathbf{v}}}{\partial y} \cdot \nabla u - \frac{\partial q}{\partial x} = \overline{v}\theta - v + \frac{\partial \mathbf{v}}{\partial y} \cdot \nabla \overline{u} + \mathbf{v} \cdot \nabla \frac{\partial \overline{u}}{\partial y}.
\end{aligned} \tag{3.3}$$

Note that on the one hand, if $\mathbf{v} = 0$, the relaxation system (3.3) reduces to

$$\begin{aligned}
&\frac{\partial u}{\partial t} - \frac{\partial \theta}{\partial x} - yv = 0,\\
&\frac{\partial v}{\partial t} + q = 0,\\
&\frac{\partial \theta}{\partial t} - \Big(\frac{\partial u}{\partial x} + \frac{\partial v}{\partial y}\Big) = 0,\\
&\frac{\partial q}{\partial t} - \frac{\partial r}{\partial x} = -\frac{\partial^2 v}{\partial y^2} + y^2 v,\\
&\frac{\partial r}{\partial t} - \frac{\partial q}{\partial x} = 0.
\end{aligned} \tag{3.4}$$

So clearly, if the system in (3.3) is solved numerically with a conservative scheme, then in the absence of a simple flow, the geostrophic balance and the zero meridional velocity of the Kelvin wave will be satisfied and preserved exactly, since if $v = q = r = 0$ at time $t = 0$, they will all remain so at all times, since their tendencies are zero at $t = 0$.

On the other hand, when the barotropic wind is reduced to a barotropic shear $\mathbf{v} = (\overline{u}(y), 0)$, the relaxation system (3.3) reads

$$\begin{aligned}
&\frac{\partial u}{\partial t} + \overline{u}\frac{\partial u}{\partial x} - \frac{\partial \theta}{\partial x} - yv = -v\frac{\partial \overline{u}}{\partial y},\\
&\frac{\partial v}{\partial t} + \overline{u}\frac{\partial v}{\partial x} + q = 0,\\
&\frac{\partial \theta}{\partial t} + \overline{u}\frac{\partial \theta}{\partial x} - \Big(\frac{\partial u}{\partial x} + \frac{\partial v}{\partial y}\Big) = 0,\\
&\frac{\partial q}{\partial t} + \overline{u}\frac{\partial q}{\partial x} - \frac{\partial \overline{u}}{\partial y}\frac{\partial \theta}{\partial x} - \frac{\partial r}{\partial x} = -\frac{\partial^2 v}{\partial y^2} + y^2 v - yv\frac{\partial \overline{u}}{\partial y},\\
&\frac{\partial r}{\partial t} + \overline{u}\frac{\partial r}{\partial x} - \frac{\partial \overline{u}}{\partial y}\frac{\partial u}{\partial x} - \frac{\partial q}{\partial x} = -v + \frac{\partial v}{\partial y}\frac{\partial \overline{u}}{\partial y} + v\frac{\partial^2 \overline{u}}{\partial y^2}.
\end{aligned} \tag{3.5}$$

It then becomes transparent that in the presence of a non-zero shear $\overline{u}(y) \neq 0$, the geostrophic balance and thus the zero-meridional velocity for the Kelvin wave will be destroyed just after a few integration-time steps through the build up of r and q because of the terms $\frac{\partial \overline{u}}{\partial y}\frac{\partial u}{\partial x}$ and $\frac{\partial \overline{u}}{\partial y}\frac{\partial \theta}{\partial x}$ respectively which feed to the tendency of v at $t = 0$, $v = r = q = 0$. Furthermore, the nature of this flux term suggests that higher-wavenumber waves and/or larger shear gradients will result in stronger deviations from meridional geostrophy and from the Kelvin wave-background solution.

3.2 Poor performance of the 2D central scheme

To discretized the relaxation system, we opt for the second order central scheme of Nessyahu and Tadmor for both its simplicity and its notoriety for handling easily and efficiently conservation laws with source terms (see [35, 48]). We use the non-staggered 2D version in [48] for conservation laws with source terms in [35], written here in the generic form

$$w_t + f(w)_x + g(w)_y = S(w).$$

Given a spacial and temporal discretization: $w(x_i, y_j, t_n) \approx w^n_{i,j}$, $x_i = i\Delta x$, $y_j = j\Delta y$ and $t_n = n\Delta t$. The non-staggered 2D central scheme in [35, 48] for this generic balance law is given by

$$\begin{aligned} w^{n+1}_{i,j} &= \frac{1}{4}(w^n_{i-1,j-1} + w^n_{i+1,j-1} + w^n_{i-1,j+1} + w^n_{i+1,j+1}) \\ &+ \frac{1}{8}(w\acute{}^n_{i-1,j-1} - w\acute{}^n_{i+1,j-1} + w\acute{}^n_{i-1,j+1} - w\acute{}^n_{i+1,j+1}) \\ &+ \frac{1}{8}(w\grave{}^n_{i-1,j-1} - w\grave{}^n_{i-1,j+1} + w\grave{}^n_{i+1,j-1} - w\grave{}^n_{i+1,j+1}) \\ &- \frac{\lambda}{4}(f(w^{n+\frac{1}{2}}_{i+1,j-1}) - f(w^{n+\frac{1}{2}}_{i-1,j-1}) + f(w^{n+\frac{1}{2}}_{i+1,j+1}) - f(w^{n+\frac{1}{2}}_{i-1,j+1})) \\ &- \frac{\mu}{4}(g(w^{n+\frac{1}{2}}_{i-1,j+1}) - g(w^{n+\frac{1}{2}}_{i-1,j-1}) + g(w^{n+\frac{1}{2}}_{i+1,j+1}) - g(w^{n+\frac{1}{2}}_{i+1,j-1})) + \frac{1}{4\Delta x\Delta y} I_s(x_i, y_j), \end{aligned} \tag{3.6}$$

where $\lambda = \frac{\Delta t}{\Delta x}$ and $\mu = \frac{\Delta t}{\Delta y}$, and the notations $(\cdot)\acute{}$ and $(\cdot)\grave{}$ represent the TVD-limited slopes in the x and y directions, respectively (see [48]). Here we use the monotone centered limiter

$$w\acute{}_{i+1,j} = \text{Min Mod}\Big\{2(w_{i+2,j} - w_{i+1,j}), \frac{1}{2}(w_{i+2,j} - w_{i,j}), 2(w_{i+1,j} - w_{i,j})\Big\}.$$

For simplicity in exposition, $w^n_{i,j}$ is used to represent both cell-averages and point-wise values. The forcing term

$$I_s(x_i, y_j) = \int_{t^n}^{t^{n+1}} \int_{x_{i-1}}^{x_{i+1}} \int_{y_{j-1}}^{x_{j+1}} S(w(x, y, t))\mathrm{d}y\mathrm{d}x\mathrm{d}t \tag{3.7}$$

is handled by the explicit scheme of [35]. Recall that the mid-point values $w^{n+\frac{1}{2}}_{i+1,j+1}$ are provided by the predictor step

$$w^{n+\frac{1}{2}}_{i,j} = w_{i,j} - \frac{\lambda}{2} f\acute{}_{i,j} - \frac{\mu}{2} g\grave{}_{i,j} + \frac{\Delta t}{2} S_{i,j}. \tag{3.8}$$

The second order derivatives are discretized by simple centered differences and incorporated into the source term. This does not seem to create any (unexpected) numerical instabilities. The resulting numerical scheme is tested for the free Kelvin wave when the barotropic shear is

zero. Up to two days of the model time, the central scheme applied to the relaxation system behaves very nicely and, as expected, the zero meridional velocity and geostrophic balance are maintained exactly. It also displays a second order convergence for the numerical error in u and θ with respect to grid refinement (results not shown here).

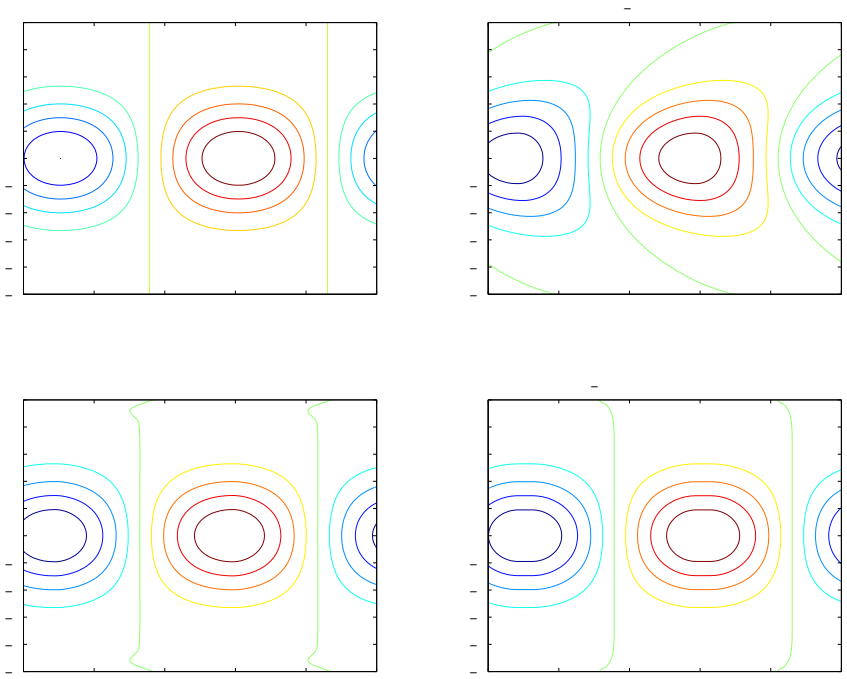

Figure 1 Contours of u at 50 days of the model run time for the Kelvin wave: Exact solution (top left), non-staggered 2D central scheme for the relaxation system (3.5) with $\overline{u} = 0$ (top right), F-wave method for the original baroclinic system (2.5) with $\overline{u} = \overline{v} = 0$ (bottom right), and non-staggered 2D central scheme for original baroclinic system (2.5) with $\overline{u} = \overline{v} = 0$ (bottom left). The grid resolution is 500×400 and a time step $\Delta t = 0.22$ hours. The axis labels are in $1,000$ km.

However, when the model is run for the long period of time of 50 days, the horizontal structure of the simulated "Kelvin wave" solution (using the 2D-central scheme) for the relaxation system (3.5) is altered significantly. The associated contours of the zonal velocity u at time $t = 50$ days, using a grid resolution of 500×400 on a periodic channel $[0, 10,000 \text{ km}] \times [-5,000 \text{ km}, 5,000 \text{ km}]$, are shown on the right top panel in Figure 1 while the left panel displays those of the exact solution. The difference is striking. After 50 days of integration time, the numerical solution adapts a heart-like shape topology. The bottom panels show the numerical solutions at the same time and with the same resolution obtained by the F-wave method of Bale et al [3] (right) and the non-staggered 2D central scheme of Nessyahu and Tadmor [48] (left) applied to the original baroclinic equations (2.5), when the barotropic wind is zero. Recall that, due to discretization errors, both these schemes show some deviations from the meridional geostrophy and therefore develop a (weak but) non-zero meridional velocity, which potentially grows with time — although not overwhelmingly with this kind of resolution. The shape of the contours of u at 50 days is captured accurately with the F-wave method and the 2D central

scheme, though the central scheme seems to suffer from a phase lag problem as it is already noticed in [26].

Presented this way, the bad performance of the first simulation could be falsely attributed to the choice of the relaxation system but a close look at this system shows that with $v = q = r = 0$ and $\theta = -u$ at $t = 0$, it reduces to the two identical one-dimensional advection equations $u_t + u_x = 0$ and $\theta_t + \theta_x = 0$, whose numerical solution, displayed in Figure 1, is clearly not the expected one. Therefore we conclude here that this bad behavior is due to the 2D central scheme, which as it is shown by the analysis below suffers from a severe distortion of the numerical speed of propagation, in the zonal direction, for the Kelvin wave so that off equatorial parts of the wave move faster that the equatorial crest. It is interesting though to notice that the same central scheme applied to the original baroclinic equations (2.5) does not seem to have this problem.

It is important to note here that the 2D Lax-Wendroff scheme (see [31]) applied to the advection equation $u_t + u_x = 0$ with the Kelvin wave initial condition (results not reported here) yielded a perfectly accurate solution at $t = 50$ days without any apparent wave distortion.

3.3 Poor dispersion properties of the 2D central scheme

Consider the simple one-dimensional advection equation

$$u_t + au_x = 0, \quad u(x, y, 0) = \beta(x)\Gamma(y), \tag{3.9}$$

where $\Gamma(y) = \mathrm{e}^{-\frac{y^2}{2}}$ represents effectively the evolution of the Kelvin wave. The advection velocity a is normalized to $a = 1$ for simplicity. Assume that the 2D non-staggered central scheme (3.6) is applied to this equation, with the minmod limiter turned off so that the xy slopes were frozen to their centered differences values $u'_{i,j} = \frac{u_{i+1,j} - u_{i-1,j}}{2}$ and $u\grave{}_{i,j} = \frac{u_{i,j+1} - u_{i,j-1}}{2}$, respectively. Notice that such assumption is not an exaggeration here since the solution is very smooth; there are no shocks. Then the central scheme for the unidirectional advection equation becomes

$$\begin{aligned} u_{i,j}^{n+1} = & \frac{1}{4}[u_{i-1,j-1}^n + u_{i-1,j+1}^n + u_{i+1,j-1}^n + u_{i+1,j+1}^n] \\ & - \frac{1}{16}[u_{i-2,j-1}^n - 2u_{i,j-1}^n + u_{i+2,j-1}^n + u_{i-2,j+1}^n - 2u_{i,j+1}^n + u_{i+2,j+1}^n \\ & + u_{i-1,j-2}^n - 2u_{i-1,j}^n + u_{i-1,j+2}^n + u_{i+1,j-2}^n - 2u_{i+1,j}^n + u_{i+1,j+2}^n] \\ & - \frac{a\lambda}{4}[u_{i+1,j-1}^n - u_{i-1,j-1}^n + u_{i+1,j+1}^n - u_{i-1,j+1}^n] \\ & + \frac{a^2\lambda^2}{16}[u_{i+2,j-1} - 2u_{i,j-1} + u_{i-2,j-1} + u_{i+2,j+1} - 2u_{i,j+1} + u_{i-2,j+1}]. \end{aligned} \tag{3.10}$$

We now consider plane wave solution for this difference scheme on the form

$$u_{ij}^n = \rho^n \mathrm{e}^{\mathrm{i}(kx_i - \omega t_n)}\Gamma(y_j) \tag{3.11}$$

with $\mathrm{i}^2 = -1$ and $\rho > 0$ is the wave amplitude, in the manner of von Neumann analysis (see [9]). Plugging this ansatz into (3.10) yields

$$\rho[\cos(w_r\Delta t) - \mathrm{i}\sin(w_r\Delta t)]\Gamma(y_j)$$

$$= \frac{1}{2}\cos(k\Delta x)[\Gamma(y_{j-1}) + \Gamma(y_{j+1})] + \frac{1}{8}[(1 - \cos(2k\Delta x))[\Gamma(y_{j-1}) + \Gamma(y_{j+1})]$$
$$- \cos(k\Delta x)[\Gamma(y_{j-2}) - 2\Gamma(y_j) + \Gamma(y_{j+2})]] - \frac{a\lambda}{2}\mathrm{i}\sin(k\Delta x)[\Gamma(y_{j-1}) + \Gamma(y_{j+1})]$$
$$+ \frac{a^2\lambda^2}{8}[(\cos(2k\Delta x) - 1)][\Gamma(y_{j-1}) + \Gamma(y_{j+1})].$$

Let $P(y_j) = \Gamma(y_{j-1}) + \Gamma(y_{j+1})$ and $Q(y_j) = \Gamma(y_{j-2}) - 2\Gamma(y_j) + \Gamma(y_{j+2})$. Let

$$W(y_j) = \frac{1}{2}\cos(k\Delta x)\Big[P(y_j) - \frac{1}{4}Q(y_j)\Big] + \frac{1}{8}P(y_j)(1 - \cos(2k\Delta x))(1 - \lambda^2)$$

and

$$V(y_j) = \frac{\lambda}{2}\sin(k\Delta x)P(y_j).$$

Then the phase speed and growth rates of the plane wave solution for the (central) difference scheme are given by

$$\frac{\omega}{k} = \frac{1}{k\Delta t}\arctan\Big(\frac{V}{W}\Big) \tag{3.12}$$

and

$$\rho = \frac{\sqrt{V^2 + W^2}}{|\Gamma(y_j)|}. \tag{3.13}$$

The y-structures of the phase speed and growth rate in (3.12) and (3.13) are plotted in Figure 2 for $\Gamma(y) = \mathrm{e}^{-\frac{y^2}{2}}$ (top panels) and $\Gamma(y) = \sin(\frac{\pi y}{5})$ (bottom panels). From the top panels we see clearly that both the growth rate and the phase for the 2D central scheme with a frozen stencil are highly dependent on y when $\Gamma(y) = \mathrm{e}^{-\frac{y^2}{2}}$ and clearly not much when $\Gamma(y) = \sin(\frac{\pi y}{5})$. On the top panels, we see that the Kelvin wave, at least initially, the central scheme will tend to damp slightly the solution at the equator and amplifies it off the equator, at the inflection points of $\mathrm{e}^{-\frac{y^2}{2}}$ while the whole structure moves at a faster speed near the equator and at a slower speed off the equator, beyond roughly the deformation-radius turning point. However, it is important to note that variations in the growth rate with latitude, between $-2,000$ km and $2,000$ km do not exceed $5/10,000$, while variation in phase speed, over the same meridional span, is on the order of $2/100$. Clearly, it must be this y-dependence of the phase speed and growth rate (and more so the phase) that are responsible for the distortion of the structure of the Kelvin wave solution in Figure 1. To help understand how the non-uniform phase speed and non-uniform growth rate distorts the Kelvin wave structure, we attempt to reconstruct the numerical solution associated with the scheme (3.10), from the plane wave ansatz in (3.11) with ρ and ω given explicitly through (3.12) and (3.13), respectively. But since the y-structure of the numerical solution changes constantly with time, this is rather a tricky game. Nevertheless, to help appreciate the individual contribution from the phase speed and growth rate separately to this wave distortion, we evolve the plane wave solution to $t_n = 50$ days, according to the iterative scheme

$$\begin{aligned} &u_{n+1}(x,y) = \beta(kx - \Delta t S_{n+1}(y))\Gamma_{n+1}(y), \quad n \geq 0,\\ &S_{n+1}(y) = \sum_{l=0}^{n}\omega_n(y), \quad \Gamma_{n+1}(y) = \prod_{l=0}^{n}\rho_l(y),\\ &u_0(x,y) = \beta(kx)\Gamma_0(y), \quad \Gamma_0(y) = \mathrm{e}^{-\frac{y^2}{2}} \end{aligned} \tag{3.14}$$

with $\omega_l, \rho_l, l \geq 0$ are given by either

(i) Varying amplification factor alone: $\rho_l(y) = \rho_0(y)$ for all $l \leq 1$, with $\rho_0(y)$ given by (3.13) with $\Gamma(y) = \Gamma_0(y) = \mathrm{e}^{-\frac{y^2}{2}}$ and $\omega_l(y) = 1$ for all $l \geq 1$,

(ii) Varying phase speed alone: $\rho_l = 1$ for all $l \geq 0$ and ω_l given by (3.12) with $\Gamma(y) = \Gamma_l(y)$ for all $n \geq 0$, or

(iii) Varying both phase speed and growth rate: $\omega_l(y)$ and $\rho_l(y)$ given respectively by (3.12) and (3.13) with $\Gamma(y) = \Gamma_l(y)$, $\forall\, l \geq 0$.

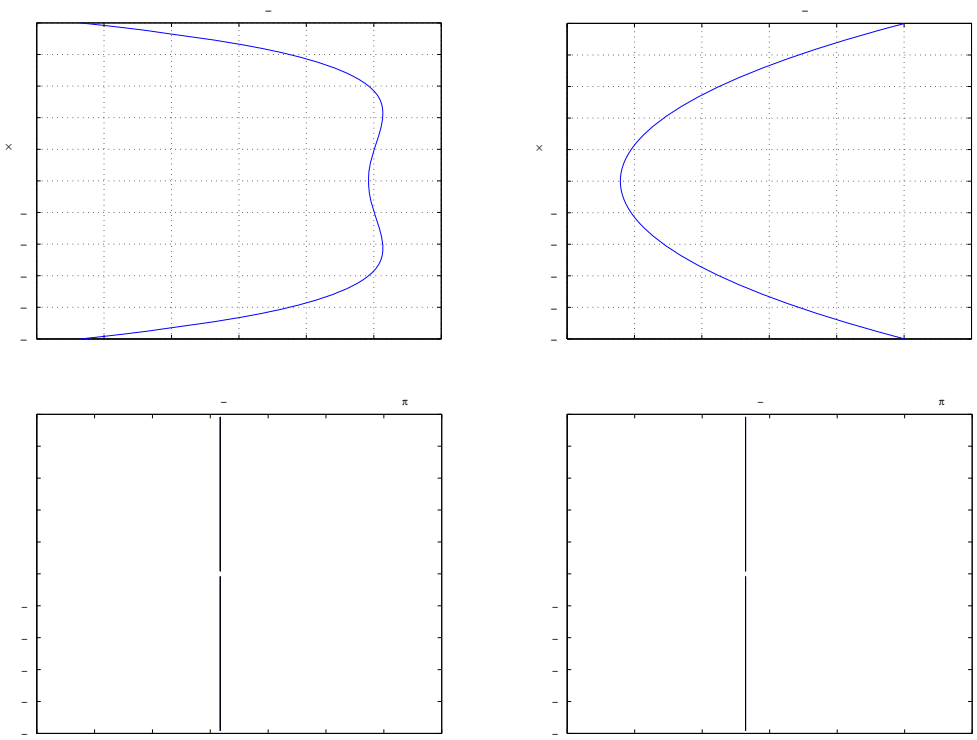

Figure 2 Phase speed (right) and growth rate (left) as functions of the distance from the equator, y, for the 2D central scheme applied to the uni-directional advection equation in (3.9) with $\Gamma(y) = \mathrm{e}^{-\frac{y^2}{2}}$ (top) and $\Gamma(y) = \sin(\frac{\pi y}{5})$ (bottom).

Notice that with Case (iii) the iterative scheme (3.14) is the one which mimics best the difference scheme in (3.10). However, we have to make a difficult choice of not including the y-dependence from the wave part of the solution, namely $\beta_n(x, y) = \beta(kx - \Delta t S_n(y))$, is not considered in the computation of ρ_n and $\omega_n(y)$.

The resulting solutions are plotted in Figure 3, with the top panel displaying the contours of $u_n(x, y)$ at $n\Delta t = 50$ days associated with Case (i) of varying the amplification factor only while the middle one corresponds to Case (ii) where only the phase speed varies, and the bottom panel is associated with Case (iii) where both ω and ρ are varied. Clearly from this picture the distortion effect due to a differential phase speed is predominant due to the fact that off equator parts of the wave move relatively faster, while the amplification factor variation with y merely expands the solution in the meridional direction due to the fact that the solution is

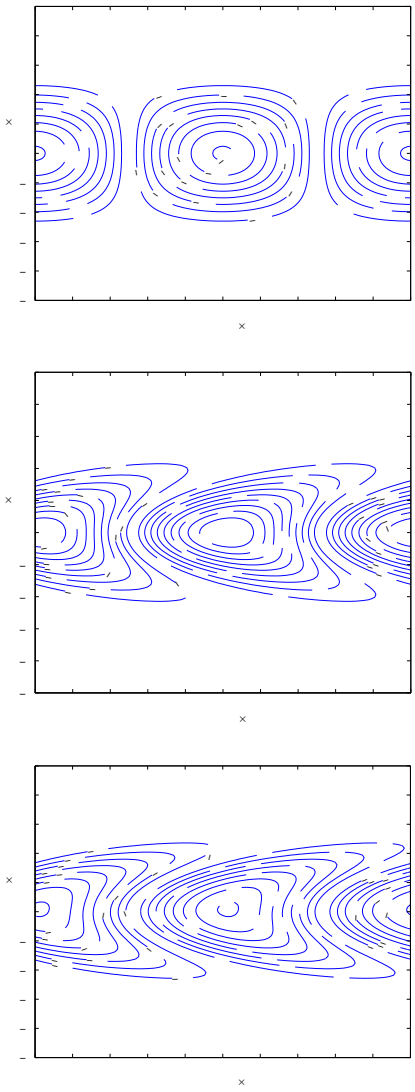

Figure 3 Contours of the wave solution $u_n(x, y)$ obtained by the iterative process (3.14) with $n = 5400$ and $\Delta t = 0.22$ hours corresponding to the solution at $t = 50$ days as in Figure 1. Top: effect of varying amplification factor alone; middle: effect of varying phase speed alone; bottom: varying amplification factor and varying phase speed combined (see text for details).

damped at the equator and amplified off the equator.

We conclude this subsection by stressing that the 2D central scheme is inadequate for equatorially trapped waves even though when applied to the original governing equations (2.4) the Kelvin wave solution at 50 days seems to be okay, probably due to some sort of compensation from the "artificial" deviation from meridional geostrophy. We anticipate here that the danger persists especially if this scheme is used to advect a tracer in a given direction that has a complex structure in the perpendicular direction. It can occur for example for moisture or liquid water fields that are associated with a convectively coupled equatorial wave, which propagate along

and are trapped in the vicinity of the equator.

3.4 Interaction of a Kelvin wave and a barotropic-meridional shear

Here we consider the baroclinic system in (2.4) forced with a stationary (fixed) barotropic shear

$$\overline{u} = U(y) = U_0(2y^2 - 1)\mathrm{e}^{-\frac{y^2}{4}}, \quad \overline{v} = 0,$$

a jet stream like mean barotropic wind (see [27]) with a mean easterly wind at equator ($y = 0$), fixed by $U(0) = -U_0$. The structure of this mean wind is illustrated in Figure 4. Note that with $U_0 = 10\ \mathrm{m} \cdot \mathrm{s}^{-1}$ the maximum westerly wind of about $25\ \mathrm{m} \cdot \mathrm{s}^{-1}$ is reached roughly at a distance $y = 2500$ km from the equator, i.e., between 20 and 25 degrees, which roughly mimics the jet stream (see [62, 64]). We propose to look at the evolution of the Kelvin wave in the presence of such a meridional shear.

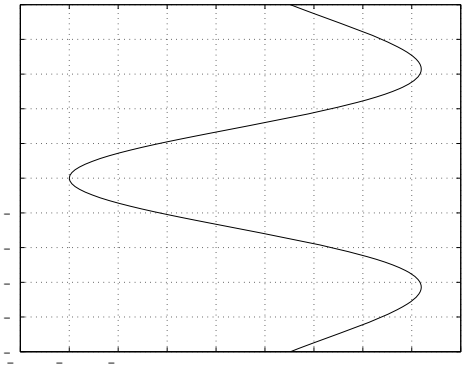

Figure 4 Mean meridional-barotropic shear used to force the Kelvin wave, with an equatorial easterly wind $U(0) = -10\ \mathrm{m} \cdot \mathrm{s}^{-1}$.

We initialize the state variables in (2.4) to the Kelvin wave solution at time $t = 0$, fix the barotropic wind to the meridional shear of Figure 4, and integrate the system numerically for a long period of time. To avoid unwanted numerical artifacts, we use the F-wave scheme of Bales [3]. The grid size is 250×200 for a periodic channel centered at the equator of width $10,000$ km (the channel walls are at $\pm 5,000$ km from the equator). The domain size in the zonal direction is set to match the wavelength of the wave, which varies from case to case. The time step is set to $\Delta t = 0.5 \min(\Delta x, \Delta y)$ to satisfy the CFL condition.

The arrow flow field and the contours of θ for the numerical solution are given on the left panels of Figure 5, while the contours of u are given on the right panels of Figure 5. In this experiment, the length of the domain is fixed to $4,000$ km corresponding to Kelvin wave with wavenumber $k = 10$. The solution is shown at roughly each days during the first 5 days of simulation. From these results, we see clearly that the interactions of the Kelvin wave with a meridional shear induces non-trivial and interesting dynamics. Both the shape of the θ and u contours and the flow fluid as a whole seem to undergo some complicated changes with an apparent oscillation of the overall deformation of about two days, which clearly can not be explained by the advection effects alone. An important aspect, relevant to convectively

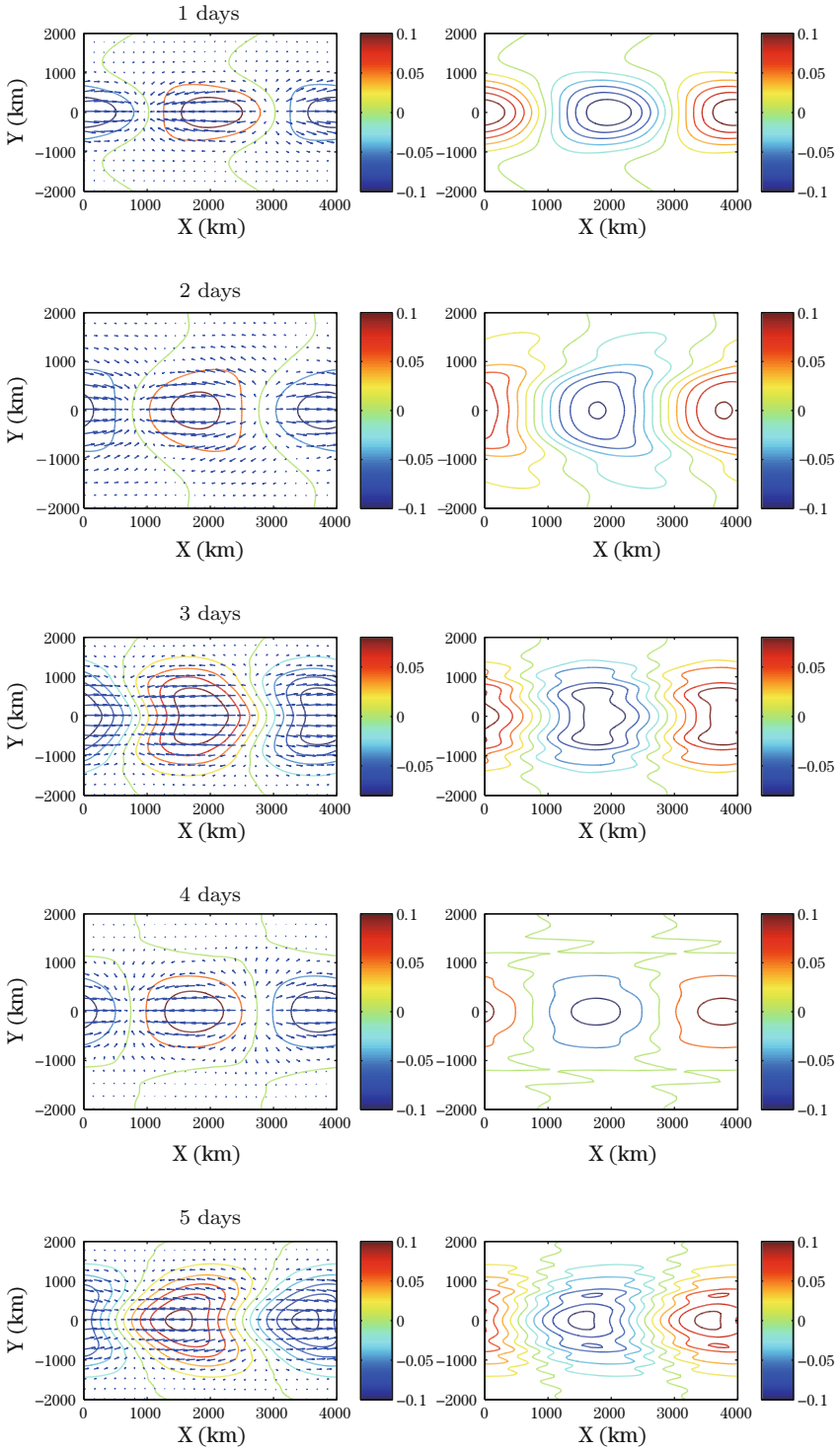

Figure 5 Flow velocity field overlaid on the contours of the potential temperature θ (left) and zonal velocity u contours (right), for the Kelvin wave forced by a meridional-barotropic wind shear with easterlies at the equator. The wave wavelength (domain size) is $4,000$ km and the solution is shown at times (from top to bottom) $t = 1$ day, $t = 2$ days, $t = 3$ days, $t = 4$ days and $t = 5$ days.

coupled waves, is the emergence of a non-zero meridional velocity and a significant meridional convergence in phase with and thus enforces the zonal convergence, i.e., the upward motion, carried by the background Kelvin wave alone.

As it is anticipated, from the relaxation system (3.5) the build up of the meridional velocity is due to the meridional shear $\overline{u}_y(y)$ and the zonal gradient of the wave $u_x(x, y, t)$, i.e., the wavenumber. In Figure 6, we show the flow structure at $t = 2$ days for three different values of the wavenumber, namely, $k = 1$, $k = 4$ and $k = 10$ (corresponding to Figure 5). Consistent with the intuition, the deformation is greater at larger wavenumbers. In Figure 7 the time series of relative meridional wind (left panels) and relative meridional convergence $\frac{\max(-v_y(x,y))}{\max(-u_x(x,y)-v_y(x,y))}$ (right panel) are plotted for three different wavenumbers $k = 1, 4, 10$ and for a total time period of 50 days. Interestingly, while the meridional velocity seems to increase significantly with increasing wavenumber, the strength of the meridional convergence exhibits roughly the same range of oscillations between 10% to 40%. Nevertheless, the period and strength of these oscillations change quite a lot with the wavenumber. With $k = 1$ and $k = 4$, we have a clear cut between low frequency oscillations of about 7 to 10 days period, superimposed on top of higher frequency modes oscillating rapidly with a period of about 1 day or so. The high frequency oscillations seem to amplify greatly as the wavenumber is increased and at $k = 10$, the low-frequency mode gets blurred and becomes somewhat indistinguishable.

An interesting question to ask is what kind of physical mechanisms are responsible for the

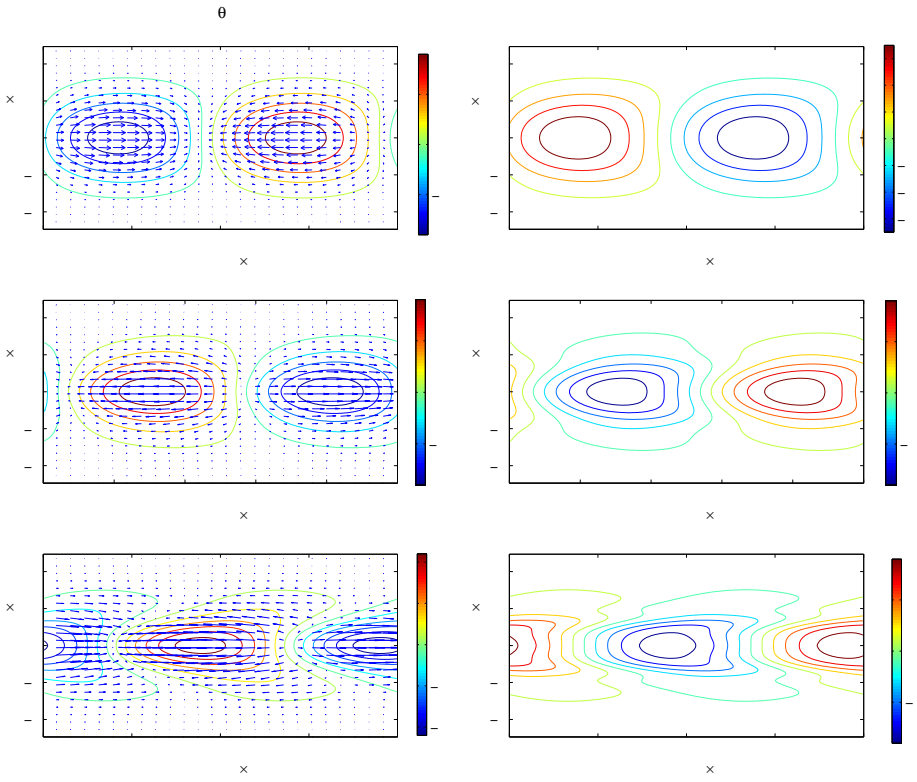

Figure 6 Same as Figure 5 but only at time $t = 2$ days and for different wavelengths: $40,000$ km (top), $10,000$ km (middle) and $4,000$ km (bottom).

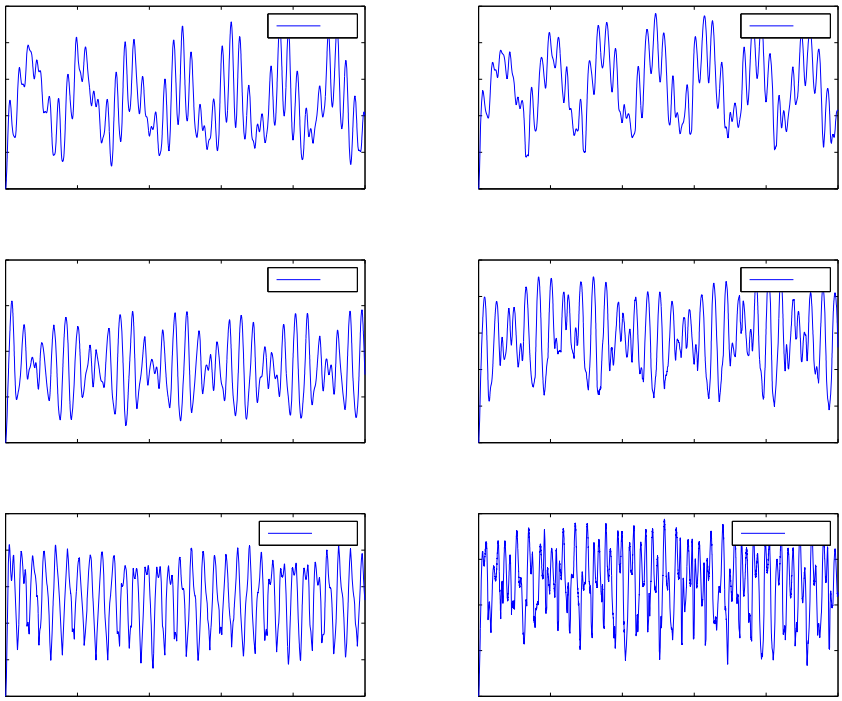

Figure 7 Time series of the relative meridional wind (left) and relative meridional convergence (right). Wavenumbers: $k = 1$ (top), $k = 4$ (middle) and $k = 10$ (bottom).

oscillations in Figures 6 and 7? Can one still represent the solution in term of the normal modes the equatorial shallow water equations? According to previous work by Webster and others [62, 64], we know that a meridional shear has very little effect on the Kelvin itself[1] and clearly what is happening here is not a simple matter of deformation by wind advection. We anticipate here that both the strong oscillations and the non-trivial meridional velocity and meridional convergence are due to the excitement of other equatorially trapped waves such as gravity waves and/or Rossby waves of different meridional indices from the interactions of the Kelvin wave and the meridional shear flow. Detailed spectral analysis, which reveal the nature of such waves possibly dependently on the wavenumber and strength of the shear, will be reported elsewhere by two of the authors.

4 The Barotropic Response to an Equatorially Trapped Kelvin Wave

In this section, we consider the barotropic equations in (2.3) with an equatorial Kelvin wave forcing. When the baroclinic flow on the right-hand side of (2.3) is fixed to the Kelvin wave flow field

$$u(x, y, t) = \alpha e^{-\frac{y^2}{2}} \cos(k_0(x - ct)), \quad v = 0,$$

[1] If we define the Kelvin wave as the simple solution with $u = -\theta$ and $v = 0$, it is easy to show (results not reported here) that such solution is supported by the meridional shear-advected equations in the frame moving with the barotropic wind.

the barotropic system in vorticity-stream function becomes

$$\begin{aligned}
&\frac{\partial\overline{\xi}}{\partial t} + J(\overline{\psi},\overline{\xi}) = \frac{k_0 y\alpha^2}{2}\mathrm{e}^{-y^2}\sin(2k_0(x-ct)),\\
&\Delta\overline{\psi} = \overline{\xi} - y,\\
&J(f,g) = f_x g_y - f_y g_x.
\end{aligned} \tag{4.1}$$

Here α sets the strength of the forcing and is chosen such that $\max|u(x,y)| = 10\ \mathrm{m}\cdot\mathrm{s}^{-1}$ while the wavenumber k_0 and the phase speed c are varied.

The system in (4.1) has many implications, in practice, as a simple model to study the direct effects of equatorially trapped Kelvin waves on the barotropic Rossby waves and possible mechanisms through which barotropic Rossby waves that can propagate North-South are exited and generated by convectively coupled equatorial waves, as seen in nature (see [51]). Here we concentrate on the latter; all other interesting issues that can be addressed by this model are left for future research.

4.1 The Arakawa Jacobian

To solve the vorticity equation (4.1), we opt here for the finite differences scheme introduced and used for climate predictions, by Arakawa [1] in the sixties, known in the geophysical community as the Arakawa-Jacobian. The starting point of the Arakawa scheme is to write the Jacobian $J(\overline{\psi},\overline{\xi})$ in three different ways, by taking advantage of the incompressibility condition

$$\begin{aligned}
J_1(x,y) &= \overline{\psi}_x\overline{\xi}_y - \overline{\psi}_y\overline{\xi}_x,\\
J_2(x,y) &= (\overline{\psi}_x\overline{\xi})_y - (\overline{\psi}_y\overline{\xi})_x,\\
J_3(x,y) &= (\overline{\psi}\,\overline{\xi}_y)_x - (\overline{\psi}\,\overline{\xi}_x)_y.
\end{aligned} \tag{4.2}$$

It is easy to see that $J(\overline{\psi},\overline{\xi}) = J_1(x,y) = J_2(x,y) = J_3(x,y)$. Consider a discretization $x_i = i\Delta x$, $y_j = j\Delta y$ for a periodic channel domain around the equator and let $\Delta t > 0$ be the time step. Let $\widehat{J}_1(i,j)$, $\widehat{J}_2(i,j)$ and $\widehat{J}_3(i,j)$ be the numerical approximations of $J_1(x,y)$, $J_2(x,y)$ and $J_3(x,y)$, respectively, obtained by approximating each one of the first order partial derivatives by centered differences. Then the Arakawa Jacobian is given by the arithmetic average

$$\widehat{J}(i,j) = \frac{1}{3}(\widehat{J}_1(i,j) + \widehat{J}_2(i,j) + \widehat{J}_3(i,j)).$$

The main strength of the Arakawa Jacobian resides in the fact that it conserves both numerical energy

$$\widehat{E}(t) = \sum_{k,l}(k^2+l^2)\widehat{\psi}_{k,l}^2$$

and numerical enstrophy

$$\widehat{\zeta}(t) = \sum_{k,l}(k^4+l^4)\widehat{\psi}_{k,l}^2,$$

where $\widehat{\psi}_{k,l}$ is the discrete Fourier transform of $\psi_{i,j}$ and k,l are the wavenumbers in the zonal (x) and meridional (y) directions, respectively. More details on the Arakawa Jacobian can be found in [1, 12].

4.2 Barotropic Rossby waves generated by a large scale Kelvin wave

Here we solve the forced barotropic equations in (4.1) using a time-operator splitting (see [26]) where the conservative part, on the right-hand side, is handled by the Arakawa Jacobian method discussed above (see [1]), combined with a hybrid Poisson solver (second order centered differences in y and spectral in x), which preserves the divergence-free constraint at the mid-points (see [26]), and a second order Runge-Kutta solver for the forcing term (see [12, 26]). We use a spacial grid of 256×150 points on a periodic channel of length $40,000$ km (the circumference of the earth at the equator) and $10,000$ km wide. We use no-flow boundary conditions ($\overline{v} = 0$) in the meridional direction-y at the channel walls and periodic in x. The time step is set by the CFL condition to roughly $\Delta t = 5$ hours, to resolve the fastest Rossby waves in the model.

We fix the parameters of the external (Kelvin wave) forcing to

$$\alpha = 10 \text{ m} \cdot \text{s}^{-1}, \quad c = 5 \text{ m} \cdot \text{s}^{-1}, \quad k_0 = \frac{2\pi}{40,000} \text{ km}^{-1}.$$

Starting with a zero initial condition $\overline{u} = \overline{v} = 0$, we integrate the forced model for 100 days and plot the energy time series $E(t)$ in Figure 8. Interestingly, the response is not trivial. Instead of a simple solution resembling the imposed forcing, the energy time series suggests a superposition of several wave-like modes that oscillate with different frequencies.

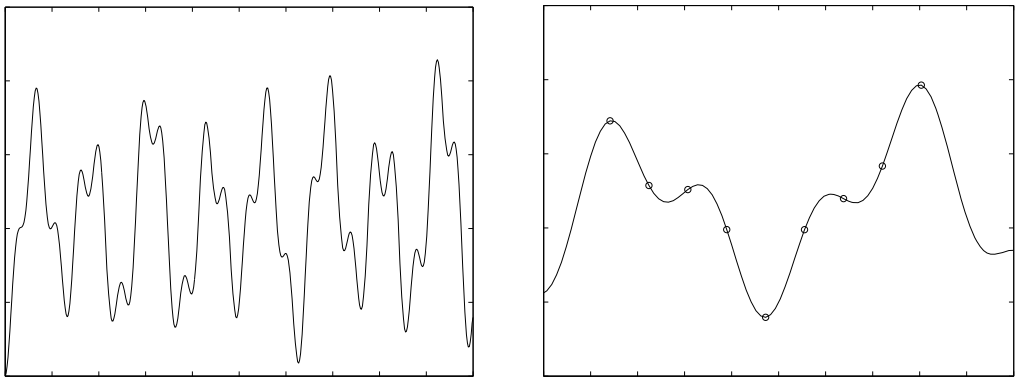

Figure 8 Energy time series for the barotropic system forced by a Kelvin wave with $\alpha = 10 \text{ m} \cdot \text{s}^{-1}$, $c = 5 \text{ m} \cdot \text{s}^{-1}$ and $k_0 = \frac{2\pi}{40,000} \text{ km}^{-1}$. The vertical axis is in non-dimensional units ($50 \times 50 \text{ J} \cdot \text{kg}^{-1}$). A zoom on a shorter period corresponding roughly to the largest period of oscillation.

A few snapshots of the stream function and the flow structure at a few successive times spanning roughly one long period of oscillation, indicated by the small circles on the right panel in Figure 8, are shown in Figure 9. We note considerable changes in topology of the solution as it evolves in time. We attribute these complex patterns to different phases of linear superpositions of waves of different wavelengths moving at different speeds. Below, we use some mathematical tools to diagnose these waves and try to understand their relationships with the imposed forcing.

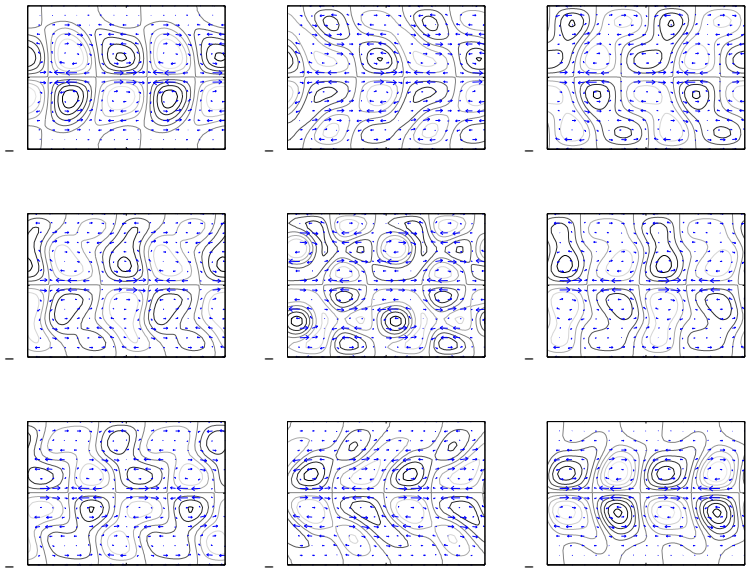

Figure 9 Level contours of the stream function and flow field arrows for the barotropic system forced by a Kelvin wave with $\alpha = 10\ \mathrm{m}\cdot\mathrm{s}^{-1}$, $c = 5\ \mathrm{m}\cdot\mathrm{s}^{-1}$ and $k_0 = \frac{2\pi}{40{,}000}\ \mathrm{km}^{-1}$ at the nine successive times indicated by the small circles on the right panel plot of Figure 8. The horizontal and vertical axises correspond to zonal and meridional directions in units of $1,000$ km.

In Figure 10, we plot the contours of the meridionally (north-south) averaged zonal wind $\overline{u}$ in the xt-plane. Such a diagram, known in the geophysical community as a Hovmuller diagram, is a useful tool for diagnosing wave-like motions in a given time series of observational or numerical simulations data. From Figure 10, streaks of waves moving in both directions along the equator are evident. Another important tool to study wave motions is Fourier analysis. In Figure 11, we plot the spectrum power obtained by the 2D Fourier transform of the meridionally averaged zonal wind shown in Figure 10. It is known, in the atmospheric science community, as the Wheeler-Kiladis diagram. From Figure 11, we distinguish three separate spectral peaks, one on the right side of $k = 0$, representing a "linear" wave moving to the east and two on the left, associated with westward moving waves. Interestingly, all these three waves have the same zonal wavenumber in magnitude, which is twice as high as that of the Kelvin wave, i.e., corresponding to that of the forcing on the right hand side of (4.1) but they have quite different frequencies. Next, we use a cut-off filter in the Fourier space based on these three spectral peaks and look at each one of these waves separately. More details on this procedure can be found in [12, 23, 24, 65].

The structure of each one of the waves that are identified and filtered from Figure 11 are represented in Figure 12. A single snapshot of the stream function is shown for each wave. The eastward moving wave is shown on the top panel, the faster westward wave in the middle, and the slower one on the bottom panel. The two westward moving waves have both the familiar structure of the barotropic Rossby waves, the solutions of (2.5) when $u = v = 0$ with a common zonal wavenumber $k = 2$ and meridional wavenumbers the full length and half the length of

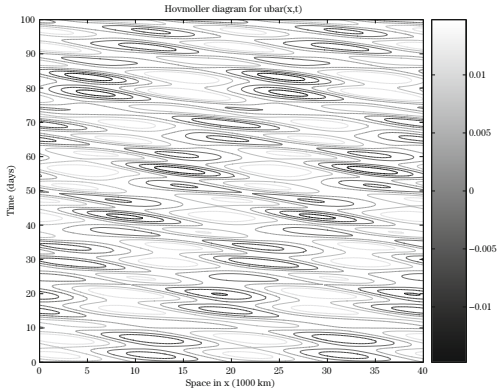

Figure 10 Hovmuller diagram of the meridionally averaged zonal wind — barotropic response to a Kelvin wave — forcing with $\alpha = 10\ \mathrm{m{\cdot}s^{-1}}$, $c = 5\ \mathrm{m{\cdot}s^{-1}}$ and $k_0 = \frac{2\pi}{40{,}000}\ \mathrm{km^{-1}}$.

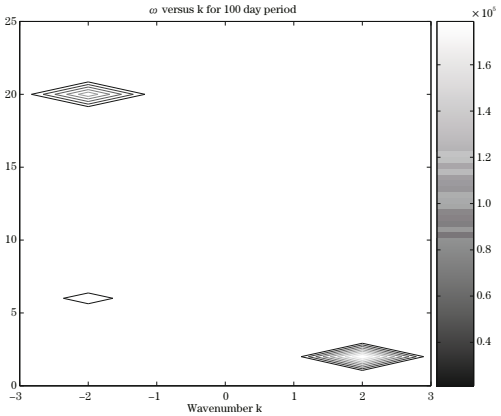

Figure 11 Spectrum power, in the wavenumber-frequency domain, of the meridionally averaged zonal wind — barotropic response to a Kelvin wave — forcing with $\alpha = 10\ \mathrm{m{\cdot}s^{-1}}$, $c = 5\ \mathrm{m \cdot s^{-1}}$ and $k_0 = \frac{2\pi}{40{,}000}\ \mathrm{km^{-1}}$.

the channel width, respectively, yielding a theoritical phase speed of about 45 $\mathrm{m \cdot s^{-1}}$ and 13 $\mathrm{m \cdot s^{-1}}$, according to the dispersion relation $\omega = -\frac{k}{k^2+l^2}$, that are roughly comparable to the values 46.30 and 13.89 $\mathrm{m \cdot s^{-1}}$, respectively, that are directly computed from the Wheeler-Kiladis diagram in Figure 11. As for the eastward moving part, we claim that it is phase-locked with the Kelvin-wave forcing.

First, its phase speed is estimated from the diagram to be about 4.63 $\mathrm{m \cdot s^{-1}}$ which is, up to a small numerical error, equal to that of the imposed Kelvin-wave forcing. Also, its meridional structure vanishes away from the equator; it is equatorially trapped. Thus, in some sense this eastward moving wave is a phase-locked wave — direct response of the barotropic equations while the westward modes are internal modes that are excited through non-linear resonant

interactions of those internal modes and the phase-looked wave.

4.3 The phase locked wave and non-linear resonant interactions

Consider the barotropic equations written in stream function alone

$$\frac{\partial \Delta\psi}{\partial t} + J(\psi, \Delta\psi) + \frac{\partial \psi}{\partial x} = F(x, y, t), \tag{4.3}$$

where the over-bar is dropped for simplicity in exposition and $F(x, y, t) = C\sin(2k_0(x - ct))y\mathrm{e}^{-y^2}$ represents the Kelvin wave forcing. Assume that the stream function ψ decomposes into a direct response ψ_0 plus a series of internal modes ψ_l, $l \geq 1$ with a zonal wavenumber $k = 2k_0$ (twice that of the forcing Kelvin wave) and meridional wavenumbers ($l \geq 1$):

$$\psi(x, y, t) = \psi_0(x, y, t) + \sum_{l=1}^{+\infty} \psi_l(x, y, t). \tag{4.4}$$

Plugging this ansatz into (4.3) yields

$$\begin{aligned}&\Big(\frac{\partial \Delta\psi_0}{\partial t} + \frac{\partial \psi_0}{\partial x} - F(x, y, t)\Big) + \Big(J(\psi_0, \Delta\psi_0) + \sum_{\substack{i,j=0 \\ i\neq j}}^{+\infty} J(\psi_i, \Delta\psi_j)\Big) \\ &+ \sum_{j=1}^{\infty} \Big(\frac{\partial \Delta\psi_j}{\partial t} + J(\psi_j, \Delta\psi_j) + \frac{\partial \psi_j}{\partial x}\Big) = 0,\end{aligned} \tag{4.5}$$

where the equation is decomposed into three natural parts. Note that the Rossby wave solutions ψ_j are exact solutions for the unforced barotropic equation and satisfy $J(\psi_i, \Delta\psi_i) = 0$.

We further assume that ψ_0 satisfies

$$\frac{\partial \Delta\psi_0}{\partial t} + \frac{\partial \psi_0}{\partial x} = F(x, y, t) \tag{4.6}$$

and takes the form (see [12])

$$\psi_0(x, y, t) = [A\cos(kx - \omega t) + B\sin(kx - \omega t)]g(y).$$

Substituting this ansatz into the last equation yields

$$\Big(g''(y) - \frac{k^2\omega + k}{\omega} g(y)\Big)(A\sin(kx - \omega t) - B\cos(kx - \omega t)) = \frac{C}{\omega}\sin(2k_0x - 2k_0ct)y\mathrm{e}^{-y^2}$$

with $k = 2k_0$ and $\omega = 2k_0c$. Then we have

$$B = 0, \quad A = \frac{C}{2k_0c} = \frac{\alpha^2}{2c}$$

and

$$g'' - \lambda^2 g = y\mathrm{e}^{-y^2}, \quad \text{where } \lambda^2 = \frac{k^2\omega + k}{\omega}.$$

With the boundary conditions $g(-\infty) = g(+\infty) = 0$, the solution to the second order differential equation for $g(y)$ is given by

$$g(y) = \frac{\sqrt{\pi}}{8}\mathrm{e}^{\frac{\lambda^2}{4}}\Big(\Big(1 - \mathrm{erf}\Big(y + \frac{\lambda}{2}\Big)\Big)\mathrm{e}^{\lambda y} - \Big(1 - \mathrm{erf}\Big(-y + \frac{\lambda}{2}\Big)\Big)\mathrm{e}^{-\lambda y}\Big),$$

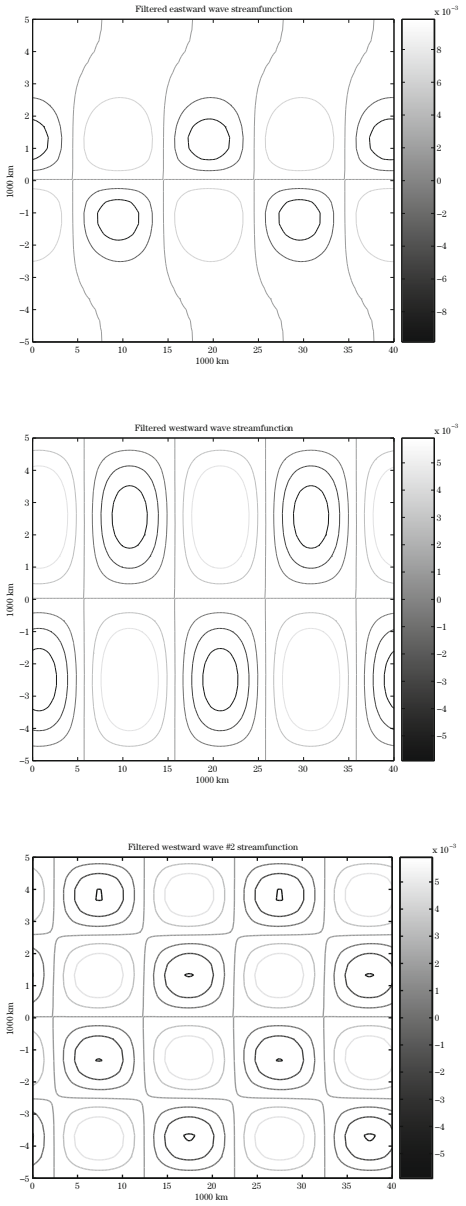

Figure 12 Contours of the filtered stream function corresponding to each one of the three spectral peaks in Figure 11. Eastward wave (top), faster westward wave (middle), slower westward wave (bottom). $\alpha = 10\ \mathrm{m \cdot s^{-1}}$, $c = 5\ \mathrm{m \cdot s^{-1}}$ and $k_0 = \frac{2\pi}{40{,}000}\ \mathrm{km^{-1}}$.

where erf is the error function

$$\mathrm{erf}(x) = \frac{2}{\sqrt{\pi}} \int_0^x \mathrm{e}^{-t^2} \mathrm{d}t.$$

The contours of the solution $\psi_0(x, y, t)$ of (4.6) are shown in Figure 13. The phase locked solution in Figure 13 compares very well in both shape and strength with the eastward wave shown on top of Figure 12, filtered from the complicated numerical solution. Therefore, we deduce that the most plausible physical scenario through which barotropic Rossby waves that can propagate poleward, i.e., teleconnection patterns, are generated by convectively coupled waves and possibly also the MJO consists in having a certain number of barotropic Rossby waves that resonate with a phase-locked barotropic response ψ_0, which is the solution of (4.6), in a way to satisfy the constraint

$$J(\psi_0, \Delta\psi_0) = -\sum_{\substack{i,j=0 \\ i \neq j}}^{\infty} J(\psi_i, \Delta\psi_j), \tag{4.7}$$

to close the equation in (4.5). Recall that each one of the Rossby wave solutions ψ_j, $j \geq 1$ is a solution for $\frac{\partial \Delta\psi_j}{\partial t} + J(\psi_j, \Delta\psi_j) + \frac{\partial \psi_j}{\partial x} = 0$.

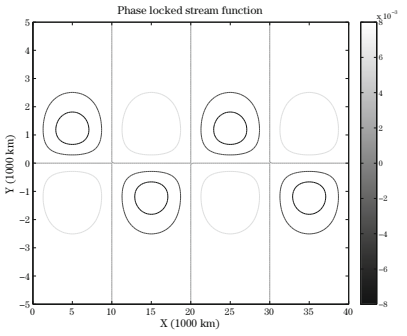

Figure 13 Contours of the phase-locked stream function ψ_0 — analytic solution of (4.6). Compare to the filtered eastward wave on the top panel of Figure 12.

The Fourier expansion of the function $g(y)$ shown in Figure 14 reveals that the phase locked wave projects mostly on the first two meridional modes, $l = 1$ and $l = 2$ (see [12]). This somewhat explains why only the two barotropic Rossby waves with the corresponding wavenumbers are visible on the Wheeler-Kiladis diagram in Figure 11. They correspond to the Rossby waves that resonate through the phase-locked response. An interesting question to address in the future is weather two or more barotropic Rossby waves alone can interact with each other and exchange energy or if such a phase-locked wave is fundamental.

We conclude this section by reporting that the same experiment was repeated with various values of the parameters k_0 and c and the same scenario was obtained at each time, i.e. the

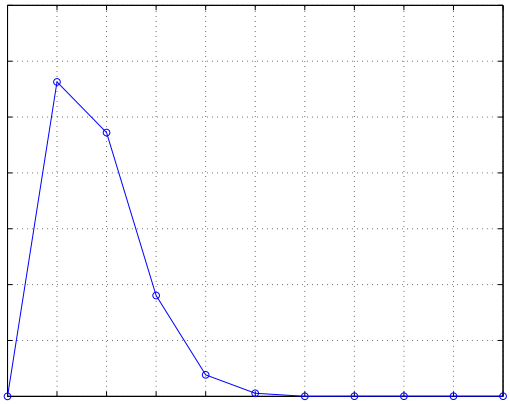

Figure 14 Power spectrum of $g(y)$ in the meridional wavenumber.

barotropic response consists of a phase-locked wave that moves together with the Kelvin wave that excites a certain number of barotropic Rossby waves with the same zonal wavenumber but different meridional wavenumbers and propagation speeds.

5 Concluding Summary and Discussion

The key issue of interactions between equatorially trapped waves and the barotropic circulation in the tropics and planetary-Rossby waves that can propagate towards the poles and excite midlatitude teleconnection patterns is examined here in the context of simplified models. Our benchmark model is the two mode barotropic (first baroclinic shallow water) like equations, first derived and used in [4, 5, 26, 27], based on a Galerkin projection of the equatorial beta-plane primitive equations on the first two modes of vertical structure. Here, we consider the two idealized situations where one of the modes is fixed and is used to force the other.

We first assume that the barotropic flow is reduced to a simple meridional shear mimicking the jet stream, and look at possible interactions between Kelvin waves and such shear flows. Given the importance of equatorially trapped waves for organized tropical convection, the understanding of the effect of a meridional and/or vertical shear on these waves was addressed in several research papers during the recent two or three decades (see [5, 62, 64, 67] and the references therein). While most of the earlier studies used linear and asymptotic analysis to look essentially at the effect of the shear on the waves, i.e., whether the wind actually changes the morphology and/or the propagation properties of these waves, here we integrate the forced system using state of art numerics to capture any deviations of the flow fields from the initially set equatorially trapped wave. The preliminary results reported here, demonstrate that the interaction of a Kelvin wave with a meridional-barotropic shear (jet stream) alters the baroclinic flow field significantly. The contours of potential temperature and velocity fields engage in an oscillatory regime going back and forth between a state where warm anomalies are leading at the equator and are lagging in the off-equatorial regions to a state where warm anomalies lead off the equator and lag at the equator. A non-zero meridional wind forms and oscillates with the whole flow structure and provides a significant equator-ward contribution to

the mass convergence in the regions of upward motion that would enhance moist convection, in the context of convectively coupled waves. While the strength of the meridional wind itself seems to increase with increasing zonal wavenumber (of the Kelvin wave), in agreement with the intuition gained from the relaxation system (3.3), the induced meridional convergence stays relatively the same regardless of the wavenumber. However, the magnitude and frequency of the oscillations in the maximum meridional wind and meridional convergence seem to amplify and change significantly with the wavenumber. At small wavenumber ($k = 1$), we distinguish two modes of oscillation, a high frequency mode with a period of about one day and a low frequency mode of about 7 days, but at high wavenumber ($k = 10$), the oscillations of the high frequency modes dominate and slow modes become indistinguishable from the time series. Since previous studies [62, 64, 67] have anticipated that a meridional shear has practically no significant effect on Kelvin waves, we argue here that both the strong oscillations and the emergence of a non-zero meridional wind must be due to the excitement of other equatorial waves through the interactions of a Kelvin wave and the fixed meridional shear. Careful Fourier analysis illustrating the nature and organization of those waves together to the extension of this work to other equatorially trapped waves will be conducted and reported elsewhere by two of the authors.

Another important issue, of practical interest, which is addressed here in the context of the Kelvin wave evolution is that of numerical schemes. It is demonstrated here that a numerical scheme whose dispersion properties depend on the direction that is perpendicular to the direction of propagation can alter artificially the morphology of the equatorially-trapped-wave fields. Therefore, such schemes should be avoided for the advection of tracers that present a complex structure in the direction perpendicular to the wind direction, such as water species in convectively coupled waves. In particular, von Neumann-like analysis revealed that the 2D central scheme of Nessyahu and Tadmor [48] tends to move the off-equatorial parts of the wave relatively faster than those at the equator, resulting in a heart like shape contours. Nevertheless, this issue can be resolved by relying on direction splitting where instead the 1D central scheme is used alternatively in each direction (see [31]).

In the second part of the paper, we investigate the response of the barotropic system (2.5) when the right hand forcing is fixed to an equatorially trapped Kelvin wave, moving along the equator at a prescribed speed varying from $c = 5\ \mathrm{m \cdot s^{-1}}$ to $c = 15\ \mathrm{m \cdot s^{-1}}$ to mimic convectively coupled Kelvin waves and the MJO in the Western Pacific warm pool region (only results with $c = 5\ \mathrm{m \cdot s^{-1}}$ are shown here). The forced barotropic system is integrated over a long period of time (100 days) and complex oscillations in the energy and the structure of the response is observed. The longest period of oscillations is about 15 days and the smallest periods are one-two days. Detailed spectral analysis reveals that the response consists essentially of three "linear" waves. One is equatorially trapped and propagates eastward with the forcing and the other two are Rossby wave — internal modes of the barotropic system, which can propagate westward and towards the pole away from the equator and excite teleconnection patterns. Interestingly, all the three waves have a zonal wavenumber twice as large as that of the Kelvin wave, consistent with the forcing.

Analytic calculations, motivated by the numerical results, suggest that such forcing induces a phase-locked barotropic wave corresponding to the eastward moving barotropic wave, which

then triggers barotropic Rossby waves through some sort of "three-way resonant interactions" satisfying

$$J(\psi_0, \Delta\psi_0) = -\sum_{i \neq j} J(\psi_i, \Delta\psi_j),$$

where ψ_0 is the phase locked response and the ψ_i's, $i \geq 1$ are the barotropic Rossby waves. It is observed here that only barotropic Rossby waves with a zonal wavenumber equal to that of the phase-locked response and the first few (two only are observed) meridional wavenumbers, on which the meridional structure of the forcing projects the most. While previous studies concentrated on the resonant interactions between barotropic and baroclinic Rossby waves (see [4, 20, 39, 61, 63]), the present work provides a plausible mechanism through which eastward convectively coupled waves generate Rossby waves that propagate poleward and in turn excite midlatitude teleconnection patterns as it occurs in nature (see [51]).

Acknowledgement Some of this work is part of M. Namazi's Ph. D. thesis and some of it is part of J. Ferguson's Master's thesis.

References

[1] Arakawa, A., Computational design for long-term numerical integration of the equations of fluid motion: Two-dimensional incompressible flow, Part I, *J. Comput. Phys.*, **1**(1), 1966, 119–143.

[2] Audusse, E, Bouchut, F., Bristeau, M.-O., et al, A fast and stable well-balanced scheme with hydrostatic reconstruction for shallow water flows, *SIAM J. Sci. Comput.*, **25**(6), 2004, 2050–2065.

[3] Bale, D. S., LeVeque, R. J., Mitran, S., et al, A wave propagation method for conservation laws and balance laws with spatially varying flux functions, *SIAM J. Sci. Comput.*, **24**(3), 2002, 955–978.

[4] Biello, J. A. and Majda, A. J., Boundary layer dissipation and the nonlinear interaction of equatorial baroclinic barotropic Rossby waves, *Geophys. Astrophys. Fluid Dyn.*, **98**(2), 2004, 85–127.

[5] Biello, J. A. and Majda, A. J., The effect of meridional and vertical shear on the interaction of equatorial baroclinic and barotropic Rossby waves, *Stud. Appl. Math.*, **112**(4), 2003, 341–390.

[6] Bond, N. A. and Vecchi, G. A., The influence of the Madden-Julian oscillation on precipitation in Oregon and Washington, *Wea. Forecasting*, **18**(4), 2003, 600–613.

[7] Bouchut, F., Sommer, J. L. and Zeitlin, V., Frontal geostrophic adjustment and nonlinear wave phenomena in one dim rotating shallow water, Part 2: high resolution numerical simulations, *J. Fluid Mech.*, **514**, 2004, 35–63.

[8] Dunkerton, T. J. and Crum, F. X., Eastward propagating ∼2- to 15-day equatorial convection and its relation to the tropical intraseasonal oscillation, *J. Geophys. Res.*, **100**(12), 1995, 25781–25790.

[9] Durran, D. R., Numerical Methods for Wave Equations in Geophysical Fluid Dynamics, Springer-Verlag, New York, 1999.

[10] Emanuel, K. A, Atmospheric Convection, Oxford University Press, Oxford, 1994.

[11] Emanuel, K. A., An air-sea interaction model of intraseasonal oscillations in the tropics, *J. Atmos. Sci.*, **44**(6), 1987, 2324–3240.

[12] Ferguson, J., A numerical solution for the barotropic vorticity equation forced by an equatorially trapped wave, Master's thesis, University of Victoria, 2008.

[13] Frierson, D. M. W., Majda, A. J. and Pauluis, O. M., Dynamics of precipitation fronts in the tropical atmosphere, *Commun. Math. Sci.*, **2**(4), 2004, 591–626.

[14] Gill, A. E., Atmosphere-Ocean Dynamics, Academic Press, New York, 1982.

[15] Hendon, H. and Liebmann, B., Organization of convection within the Madden-Julian oscillation, *J. Geophys. Res.*, **99**(4), 1994, 8073–8083.

[16] Houze, R. A., Jr., Stratiform precipitation in regions of convection: A meteorological Paradox? *Bull. Amer. Meteor. Soc.*, **78**(10), 1997, 2179–2196.

[17] Johnson, R. H., Rickenbach, T. M., Rutledge, S. A., et al, Trimodal characteristics of tropical convection, *J. Climate.*, **12**(8), 1999, 2397–2418.

[18] Jones, C., Waliser, D. E., Lau, K. M., et al, The Madden-Julian oscillation and its impact on Northern hemisphere weather predictability, *Mon. Wea. Rev.*, **132**(6), 2004, 1462–1471.

[19] Hoskins, B. J. and Jin, F.-F., The initial value problem for tropical perturbations to a baroclinic atmosphere, *Quart. J. Roy. Meteor. Soc.*, **117**(498), 1991, 299–317.

[20] Kasahara, A. and Dias, P. S., Response of planetary waves to stationary tropical heating in a global atmosphere with meridional and vertical shear, *J. Atmos. Sci.*, **43**(18), 1986, 1893–1912.

[21] Khouider, B. and Majda, A. J., A simple multicloud parametrization for convectively coupled tropical waves, Part I: linear analysis, *J. Atmos. Sci.*, **63**(4), 2006, 1308–1323.

[22] Khouider, B. and Majda, A. J., Model multicloud parametrizations with crude vertical structure, *Theor. Comput. Fluid Dyn.*, **20**(5–6), 2006, 351–375.

[23] Khouider, B. and Majda, A. J., A simple multicloud parametrization for convectively coupled tropical waves, Part II: nonlinear simulations, *J. Atmos. Sci.*, **64**(2), 2007, 381–400.

[24] Khouider, B. and Majda, A. J., Multicloud models for tropical convection: enhanced congestus heating, *J. Atmos. Sci.*, **65**(3), 2008, 895–914.

[25] Khouider, B. and Majda, A. J., Equatorial convectively coupled waves in a simple multicloud model, *J. Atmos. Sci.*, **65**(11), 2008, 3376–3397.

[26] Khouider, B. and Majda, A. J., A non-oscillatory balanced scheme for an idealized tropical climate model, Part I: algorithm and validation, *Theor. Comput. Fluid Dyn.*, **19**(5), 2005, 331–354.

[27] Khouider, B. and Majda, A. J., A non-oscillatory balanced scheme for an idealized tropical climate model, Part II: nonlinear coupling and moisture effects, *Theor. Comput. Fluid Dyn.*, **19**(5), 2005, 355–375.

[28] Kiladis, G. N., Straub, K. H. and Haertel, P. T., Zonal and vertical structure of the Madden-Julian oscillation, *J. Atmos. Sci.*, **62**(8), 2005, 2790–2809.

[29] Kiladis, G. N., Wheeler, M. C., Haertel, P. T., et al, Convectively coupled equatorial waves, *Rev. Geophys.*, **47**, 2009, RG2003. DOI:10.1029/2008RG000266

[30] Lau, W. K. M. and Waliser, D. E., Intraseasonal Variability in the Atmosphere-Ocean Climate System, Praxis, Chichester, 2005.

[31] LeVeque, R. J., Finite Volume Methods for Hyperbolic Problems, Cambridge University Press, Cambridge, 2002.

[32] Lin, J.-L., Kiladis, G. N., Mapes, B. E., et al, Tropical intraseasonal variability in 14 IPCC AR4 climate models, Part 1: convective signals, *J. Climate*, **19**(12), 2006, 2665–2690.

[33] Lin, J.-L., Lee, M.-I., Kim, D., et al, The impacts of convective parameterization and moisture triggering on AGCM-simulated convectively coupled equatorial waves, *J. Climate*, **21**(5), 2008, 883–909.

[34] Lin, X. and Johnson, R. H., Kinematic and thermodynamic characteristics of the flow over the Western Pacific Warm Pool during TOGA COARE, *J. Atmos. Sci.*, **53**(5), 1996, 695–715.

[35] Liotta, S. F., Romano, V. and Russo, G., Central schemes for systems of balance laws, Hyperbolic Problems: Theory, Numerics, Applications, Seventh International Conference in Zürich, February 1998, M. Fey and R. Jeltsch (eds.), International Series on Numerical Mathematics, **130**, Birkhäuser, Boston, 1999, 651–660.

[36] Madden, R. A. and Julian, P. R., Description of global scale circulation cells in tropics with a 40–50 day period, *J. Atmos. Sci.*, **29**(6), 1972, 1109–1123.

[37] Madden, R. A. and Julian, P. R., Observations of the 40–50 day tropical oscillation — A review, *Mon. Wea. Rev.*, **122**(5), 1994, 814–837.

[38] Majda, A. J., Introduction to PDEs and Waves for the Atmosphere and Ocean, Courant Lecture Notes, **9**, AMS, 2003.

[39] Majda, A. J. and Biello, J. A., The nonlinear interaction of barotropic and equatorial baroclinic Rossby waves, *J. Atmos. Sci.*, **60**(15), 2003, 1809–1821.

[40] Majda, A. J., Khouider, B., Kiladis, G. N., et al, A model for convectively coupled tropical waves: Nonlinearity, rotation, and comparison with observations, *J. Atmos. Sci.*, **61**(17), 2004, 2188–2205.

[41] Majda, A. J. and Shefter, M. G., Waves and instabilities for model tropical convective parameterizations, *J. Atmos. Sci.*, **58**(8), 2001, 896–914.

[42] Mapes, B. E., Convective inhibition, subgridscale triggering energy, and stratiform instability in a toy tropical wave model, *J. Atmos. Sci.*, **57**(10), 2000, 1515–1535.

[43] Matsuno, T., Quasi-geostrophic motions in the equatorial area, *J. Meteor. Soc. Japan*, **44**(1), 1966, 25–43.

[44] Moncrieff, M. W. and Klinker, E., Organized convective systems in the tropical western Pacific as a process in general circulation models: a TOGA-COARE case study, *Quart. J. Roy. Meteor. Soc.*, **123**(540), 1997, 805–827.

[45] Nakazawa, T., Tropical super clusters within intraseasonal variations over the western Pacific, *J. Meteor. Soc. Japan*, **66**(6), 1988, 823-839.

[46] Neelin, J. D., and Yu, J.-Y., Modes of tropical variability under convective adjustment and Madden-Julian oscillation, Part I: analytical theory, *J. Atmos. Sci.*, **51**(13), 1994, 1876–1894.

[47] Neelin, J. D. and Zeng, N., A quasi-equilibrium tropical circulation model-formulation, *J. Atmos. Sci.*, **57**(11), 2000, 1741–1766.

[48] Nessyahu, H. and Tadmor, E., Non-oscillatory central differencing for hyperbolic conservation laws, *J. Comput. Phys.*, **87**(2), 1990, 408–463.

[49] Raymond, D. J., A new model for the Madden-Julian oscillation, *J. Atmos. Sci.*, **58**(18), 2001, 2807–2819.

[50] Pedlosky, J., Geophysical Fluid Dynamics, Springer-Verlag, New York, 1979.

[51] Roundy, P., Analysis of convectively coupled Kelvin Waves in the Indian Ocean MJO, *J. Atmos. Sci.*, **65**(4), 2008, 1342–1359.

[52] Slingo, J. M, Sperber, K. R., Boyle, J. S., et al, Intraseasonal oscillation in 15 atmospheric general circulation models: results from an AMIP diagnostic subproject, *Climate Dyn.*, **12**(5), 1996, 325–357.

[53] Smith, R. K., The Physics and Parameterization of Moist Atmospheric Convection, Kluwer, Dordresht, 1997.

[54] Scinocca, J. F. and McFarlane, N. A., The variability of modeled tropical precipitation, *J. Atmos. Sci.*, **61**(16), 2004, 1993–2015.

[55] Straub, K. H. and Kiladis, G. N., The observed structure of convectively coupled Kelvin waves: Comparison with simple models of coupled wave instability, *J. Atmos. Sci.*, **60**(14), 2003, 1655–1668.

[56] Stechmann, S., Majda, A. and Khouider, B., Nonlinear dynamics of hydrostatic internal gravity waves, *Theor. Comput. Fluid Dyn.*, **22**(6), 2008, 407–432.

[57] Takayabu, Y. N. and Murakami, M., The structure of super cloud clusters observed in 1-20 June 1986 and their relationship to easterly waves, *J. Meteor. Soc. Japan*, **69**(1), 1991, 105–125.

[58] Takayabu, Y. N., Large-scale cloud disturbances associated with equatorial waves, Part I: spectral features of the cloud disturbances, *J. Meteor. Soc. Japan*, **72**(3), 1994, 433–448.

[59] Yano, J.-I., Moncrieff, M. W. and McWilliams, J. C., Linear stability and single-column analyses of several cumulus parametrization categories in a shallow-water model, *Quart. J. Roy. Meteor. Soc.*, **124**(547), 1998, 983–1005.

[60] Wang, B. and Xie, X. S., Low-frequency equatorial waves in vertically sheared zonal flow, Part I: stable waves, *J. Atmos. Sci.*, **53**(3), 1996, 449–467.

[61] Webster, P. J., Response of the tropical atmosphere to local steady forcing, *Mon. Wea. Rev.*, **100**(7), 1972, 518–541.

[62] Webster, P. J. and Chang, H.-R., Energy accumulation and emanation regions at low latitudes: Impacts of a zonally varying basic state, *J. Atmos. Sci.*, **45**(5), 1988, 803–829.

[63] Webster, P. J., Seasonality of atmospheric response to sea-surface temperature anomalies, *J. Atmos. Sci.*, **39**(1), 1982, 41–52.

[64] Webster, P. J. and Holton, J. R., Cross-equatorial response to middle-latitude forcing in a zonally varying basic state, *J. Atmos. Sci.*, **39**(4), 1982, 722–733.

[65] Wheeler, M. and Kiladis, G. N., Convectively coupled equatorial waves: Analysis of clouds and temperature in the wavenumber-frequency domain, *J. Atmos. Sci.*, **56**(3), 1999, 374–399.

[66] Wheeler, M., Kiladis, G. N. and Webster, P. J., Large-scale dynamical fields associated with convectively coupled equatorial waves, *J. Atmos. Sci.*, **57**(5), 2000, 613–640.

[67] Zhang, C. D. and Webster, P. J., Laterally forced equatorial waves in mean zonal flows, Part I: stationary transient forcing, *J. Atmos. Sci.*, **49**(7), 1992, 585–607.

[68] Zhang, C. D., Madden-Julian oscillation, *Rev. Geophys.*, **43**, 2005, RG2003. DOI:10.1029/2004RG000158.